

**DETERMINE THE MECHANICAL PROPERTIES OF ARTICULAR
CARTILAGE USING INDENTATION TESTING**

by

Xingyu Chen

A thesis submitted to the Faculty of the University of Delaware in partial fulfillment of the requirements for the degree of Master of Science in Mechanical Engineering

Spring 2016

© 2016 Xingyu Chen
All Rights Reserved

ProQuest Number: 10156507

All rights reserved

INFORMATION TO ALL USERS

The quality of this reproduction is dependent upon the quality of the copy submitted.

In the unlikely event that the author did not send a complete manuscript and there are missing pages, these will be noted. Also, if material had to be removed, a note will indicate the deletion.



ProQuest 10156507

Published by ProQuest LLC (2016). Copyright of the Dissertation is held by the Author.

All rights reserved.

This work is protected against unauthorized copying under Title 17, United States Code
Microform Edition © ProQuest LLC.

ProQuest LLC.
789 East Eisenhower Parkway
P.O. Box 1346
Ann Arbor, MI 48106 - 1346

**DETERMINE THE MECHANICAL PROPERTIES OF ARTICULAR
CARTILAGE USING INDENTATION TESTING**

by

Xingyu Chen

Approved: _____
X. Lucas Lu, Ph.D.
Professor in charge of thesis on behalf of the Advisory Committee

Approved: _____
Suresh G. Advani, Ph.D.
Chair of the Department of Mechanical Engineering

Approved: _____
Babatunde A. Ogunnaike, Ph.D.
Dean of the College of Engineering

Approved: _____
Ann L. Ardis, Ph.D.
Senior Vice Provost for Graduate and Professional Education

ACKNOWLEDGMENTS

First of all, I want to thank my advisor, Prof. X. Lucas Lu. With a systematic understanding of cartilage biomechanics, he offers me great guidance in stepping into this area. Under his advisory, I have avoided many potential pitfalls in my research projects. His continuous and encouraging support makes the research both fun and rewarding. I could not have accomplished this thesis without his help.

Besides, I would like to thank Prof. Liyun Wang and Prof. Michael H. Santare, from the University of Delaware and Prof. Leo. Q. Wan from Rensselaer Polytechnic Institute for being my thesis committee and their great comments on my thesis.

I thank my fellow labmates: Brandon K. Zimmerman, Leonardo Ruggiero, Michael Furr, Mengxi Lv, Miri Park and Yilu Zhou, for their technical assistance in the experiments. They also make my life at graduate school much more fun.

Last but not the least, I would like to express my deepest sense of gratitude to my parents who are always considerate, encouraging and supportive no matter what. Thank you.

TABLE OF CONTENTS

LIST OF TABLES	vi
LIST OF FIGURES	vii
ABSTRACT	x
Chapter	
1 INTRODUCTION	1
2 REVIEW OF LITERATURES	5
3 USING PRINCIPAL COMPONENT ANALYSIS TO SHORTEN THE INDENTATION TESTING TIME	10
3.1 Introduction	10
3.2 Method	10
3.2.1 Experiments	10
3.2.2 Principal component analysis	11
3.2.3 Accuracy of predicted data	12
3.3 Results	13
3.4 Discussion	18
4 DETERMINING THE TENSION-COMPRESSION NONLINEAR MECHANICAL PROPERTIES WITH FINITE ELEMENT ANALYSIS	20
4.1 Introduction	20
4.2 Method	20
4.2.1 Experiment	20
4.2.2 Nonlinear constitutive models	21
4.2.3 Optimization algorithm	23
4.3 Results	29
4.4 Discussion	33
5 SUMMARY AND FUTURE DIRECTIONS	38
5.1 Summary	38
5.2 Future directions	38
REFERENCES	40

Appendix

A	VERIFICATION OF THE NONLINEAR MODELS	44
A.1	Experimental verification of the predictive ability of the nonlinear models	44
A.2	Comparison with standard heuristic optimization method	46
B	METHOD FOR COMPARING THE PRINCIPAL COMPONENTS.....	48
B.1	Two factors in PCA prediction accuracy.....	48
B.2	Comparison between principal components from two groups of samples	50
B.2.1	Method.....	50
B.2.1.1	Create observations	51
B.2.1.2	Calculate the F-ratio	51
B.2.1.3	Comparison.....	52
B.2.2	Results	52
B.2.2.1	Comparison between TMJ and knee joint samples	52
B.2.2.2	Comparison between randomly divided TMJ samples	53
B.2.2.3	Comparison between healthy and degenerated Knee joint samples	54
B.2.3	Predict the regional difference in mechanical properties on articular cartilage	56

LIST OF TABLES

Table 3.1	Mechanical properties determined by BLE, CLE, and CFD models (*: different from CFD; +: different from CLE).	31
Table A.1	The number of evaluations and compressive modulus obtained by two optimization methods are compared.....	46
Table B.1	Paired t-test results of three groups: anterior & central, lateral & central, anterior and medial.	58

LIST OF FIGURES

Figure 2.1	Schematic representation of the collagen network interacting with the proteoglycan network, forming a porous solid matrix in articular cartilage. From Lu [29], with permission.....	5
Figure 2.2	A schematic diagram of indentation test. From Lu [29], with permission.	7
Figure 2.3	An indentation creep curve fitted by nonlinear (left) and linear (right) elastic biphasic models.....	8
Figure 3.1	Contribution of principal components to the total variance of indentation creep curves. The first principal component (<i>PCI</i>) explains 98.5% and 99.8% of the total variance for TMJ cartilage and knee joint cartilage, respectively. The third principal component contributes less than 0.5%.	14
Figure 3.2	Average principal components of 50 random combinations of 5 indentation creep curves for (a) TMJ condylar cartilage and (b) knee joint cartilage. The first principal component (<i>PCI</i>) of any five creep curves remains highly consistent with low standard deviations at all time. The second principal component (<i>PC2</i>) is not as consistent as <i>PCI</i>	14
Figure 3.3	PCA predicted indentation creep curves of two samples for each type of cartilage, using the experimental data in the first 600 seconds. The corresponding full experimental curves are also plotted for comparison.	15
Figure 3.4	The PCA predication errors are correlated with the number of full tests used for <i>PC</i> matrix construction and the length of initial testing data available for predication.	16
Figure 3.5	Comparison of mechanical properties determined by indentation curve-fitting using experimental and PCA predicted curves, (a-b) aggregate modulus, (c-d) permeability, and (e-f) shear modulus. Line $Y=X$ is plotted for reference.....	17

Figure 3.6	The difference of aggregate modulus determined from predicted and experimental data is plotted against their average value. For most samples, the difference is smaller than 5% of the average value, and the mean of the difference is close to zero (-0.003Mpa for TMJ and 0.012Mpa for knee). In addition, the difference between two data sets is not dependent on their average values. All these factors indicate that the two data sets have a good agreement.	18
Figure 4.1	A one-degree wedge of cartilage and indenter is meshed and analyzed based on the axial symmetric nature of indentation tests. The bottom of the cartilage is impermeable and fixed in all directions to mimic the cartilage-bone interface. Deformation of the contact surface is associated with the movement of the indenter tip, and the fluid pressure is set to be zero (porous indenter). u_x , u_y , and u_z represent the displacement in x , y , and z directions, respectively, and P is the fluid pressure.....	23
Figure 4.2	(a) A typical indentation creep curve from tests on bovine knee cartilage and the definition of three curve-related parameters, including the initial jump, equilibrium deformation, and half deformation time. (b) When the equilibrium deformation and half-deformation time are fixed, the initial jump of the curve is regulated by the fiber modulus.....	25
Figure 4.3	Roles of each individual mechanical property in shaping the indentation creep curve in biphasic CLE model. Creep curves are plotted by varying one of the three properties in the physiological range and keeping the other two constant (compressive modulus = 2MPa, fiber modulus = 2MPa, permeability = $0.001\text{mm}^4\cdot\text{N}^{-1}\cdot\text{s}^{-1}$): (a) compressive modulus, (b) permeability, and (c) fiber modulus. (d-f) Monotonic correlations between the mechanical properties and the deformation ratio, half deformation time, and equilibrium deformation are observed.....	25
Figure 4.4	The optimization scheme involves two levels of binary search. At the lower level, given a fiber modulus, the compressive modulus and permeability are optimized to fit the equilibrium deformation and half deformation time of the curve. At the higher level, the fiber modulus is searched to match the deformation ratio. Adjustment of fiber modulus requires a new search of compressive modulus and permeability.....	28

Figure 4.5	(a) Typical indentation creep displacement history of adult bovine knee cartilage and the curve-fittings based on BLE and biphasic CLE and CFD models. (b) Typical searching process for fiber modulus ζ . The dashed lines are simulated curves over different ζ values after fixing equilibrium deformation and half deformation time.....	30
Figure 4.6	Correlations between mechanical properties determined by biphasic CLE and CFD models. (a) Aggregate modulus, (b) permeability, and (c) fiber modulus.	32
Figure 4.7	(a) Aggregate modulus and (b) permeability obtained from CLE and CFD models are linearly correlated with those from the BLE model.	32
Figure 4.8	Curve-fitting is performed with different Poisson's ratios of the ground matrix on a single creep curve, and its effect on the determined mechanical properties is plotted. All the mechanical properties are normalized by their maximum value.	33
Figure A.1	Creep curves generated by 150 mN load were first fitted, and the response of cartilage under 50mN load was predicted with the parameters obtained through curve-fitting	44
Figure B.1	The PCA predication errors are correlated with the number of full tests used for PC matrix construction and the length of initial testing data available for predication.	49
Figure B.2	Distribution histogram of the 1000 mixed F_{π} . The average of F ratio is around 100.....	53
Figure B.3	Distribution histogram of 1000 mixed F_{π}	54
Figure B.4	The first principal component (PC1) of indentation creep curves from healthy and degenerated bovine knee cartilage.....	55
Figure B.5	Distribution histogram of 1000 mixed F_{π} for the comparison between healthy and degenerated knee joint samples	56
Figure B.6	Aggregate modulus from the TMJ indentation test data presented in [28]. The moduli were obtained by biphasic curve-fitting the full experimental data and PCA predicted creep data.....	58

ABSTRACT

Indentation testing is widely used to determine the *in situ* biomechanical properties of articular cartilage, however, most curve-fitting solutions for indentation analysis require the deformation data of cartilage at the equilibrium state, which often takes the tissue hours to reach. The lengthy testing time reduces the efficiency of indentation, increases the chance of tissue deterioration, and prevents *in vivo* applications. Moreover, the constitutive models often involve multiple parameters. Determination of all mechanical properties by curve-fitting the indentation creep data is often complicated by over-fitting, local minima and multiple solutions. This thesis aimed to address these two particular problems. First, in order to shorten the indentation testing time, a novel technique based on principal component analysis (PCA) was developed, which can predict the full indentation creep curve based on the deformation data in a short time period. Second, by identifying the role of each mechanical property in the indentation response of cartilage, a highly efficient curve-fitting algorithm was designed, which can uniquely determine the nonlinear mechanical properties of cartilage (compressive modulus, tensile modulus, and permeability) from a single indentation creep curve. Both of these two newly developed techniques have shown high accuracy and efficiency.

Chapter 1

INTRODUCTION

Indentation testing is a commonly-used technique to determine the mechanical properties of articular cartilage, as it is site-specific, non-destructive, and suitable for testing of small joints with a limited amount of tissue [1-4]. To obtain mechanical properties from indentation data, a specific constitutive model has to be employed to describe the cartilage mechanical behavior and its response under indentation test. Due to the complexity of the boundary conditions, theoretical indentation solutions can be difficult to develop, especially for comprehensive constitutive models [5]. When cartilage is treated as a linear elastic material, the Hertzian contact solution on an infinite half space is widely used, which is specifically suitable for nano- or micro-indentation tests [6]. For larger-scale indenters, Hayes solution [1] is often used since it removes the infinite half-space assumption in the Hertzian contact problem. In the early 1980's, Mow and coworkers [7] developed a porous elastic model for articular cartilage. An indentation solution was also developed based on the theory [8, 9]. Using this theoretical solution, a curve-fitting algorithm was established that can simultaneously determine the Young's modulus, shear modulus, and permeability of the cartilage from a single indentation creep curve [9]. Besides these closed-form solutions, many other numerical solutions for cartilage indentation have been developed to account for the variety of experimental parameters, such as the geometry

of the indenter tip and the loading profile [10-14]. All of these linear solutions have been widely-used to extract the biomechanical properties of cartilage from indentation tests [3, 4, 12, 15-17].

The mechanical behavior of the cartilage's solid matrix itself is nonlinear and strain-dependent due to the nature of the collagen networks and trapped proteoglycans. In particular, the tensile modulus of cartilage is found to be an order of magnitude higher than the compressive modulus [18, 19]. A few tension-compression nonlinear constitutive models have been proposed to account for this, including a conewise linear elastic (CLE) model with cubic symmetry and several fibril reinforced models [20-22]. Simulations based on these models show that the prominent nonlinearity in the stress-strain relationship of the solid matrix regulates the flow-dependent viscosity and is therefore an essential characteristic of the transient mechanical behavior [22, 23]. A few recent studies have analyzed indentation or nano-indentation tests using these nonlinear constitutive models [24-26]. However, since these nonlinear models typically contain multiple parameters, determination of all the relevant cartilage properties by curve-fitting a single indentation curve is often complicated by over-fitting, local minima, and multiple solutions [27]. For instance, to avoid local minima, multiple optimizations are often performed with different initial guesses of the tissue properties. However, little knowledge is available about the different roles of each individual mechanical property in shaping the creep behavior of cartilage, or whether these features can benefit or accelerate the curve-fitting algorithm. Indeed, no strategies are currently available that can uniquely determine the tensile and

compressive properties of cartilage based on a single indentation test. Moreover, most of these solutions for indentation require the equilibrium deformation data for curve-fitting since the deformation-load correlation at equilibrium stage (with no fluid flow) can be defined by the closed-form Hayes solution [1]. Due to the significant viscoelastic behaviors of cartilage, however, it may take up to several hours for the tissue to reach a final steady state, where the required time depends upon the loading profile, indenter tip, indentation geometry, and the biomechanical properties of the cartilage [10, 12, 13]. Such a long testing time reduces the efficiency of indentation and hinders *in vivo* applications. For example, creep testing of five regions on a small animal joint could take a dozen hours [28], which considerably increases the possibility of tissue degeneration during testing.

In this thesis, two particular problems in current methods are discussed and addressed. First, to shorten the indentation testing time, a data processing technique was developed using principal component analysis (PCA) to predict the full indentation creep curve based on the transient data obtained in the first few minutes of indentation testing. The accuracy of the prediction was verified using experimental data from two types of articular cartilage, bovine knee cartilage and condylar cartilage from the porcine temporomandibular joint (TMJ). Second, a highly efficient algorithm was developed to uniquely determine the nonlinear biphasic properties of cartilage from a single indentation creep test uniquely. This new algorithm was then applied to analyze experimental data from adult bovine knee cartilage. The results were validated by comparison with the classical biphasic linear elastic program.

In this thesis, Chapter 2 reviews the major technique developments in indentation analysis. Chapter 3 presents the technique developed to shorten the indentation testing time. Chapter 4 presents the algorithm to determine the tension-compression nonlinear mechanical properties of cartilage. Chapter 5 summarizes the thesis work and discusses the potential future directions.

Chapter 2

REVIEW OF LITERATURES

Articular cartilage is a thin layer of soft tissue that covers the bony ends in diarthrodial joints and functions as a cushion to provide load support with almost no friction. From an engineering perspective, the tissue is a porous collagen matrix (15-22% wet weight) filled with water and proteoglycans (4-7% wet weight) [29] as shown in Fig. 2.1. Studying the mechanical behaviors of the articular cartilage is very critical for understanding the degeneration of the tissue during diseases as pointed out by Mow in [30].

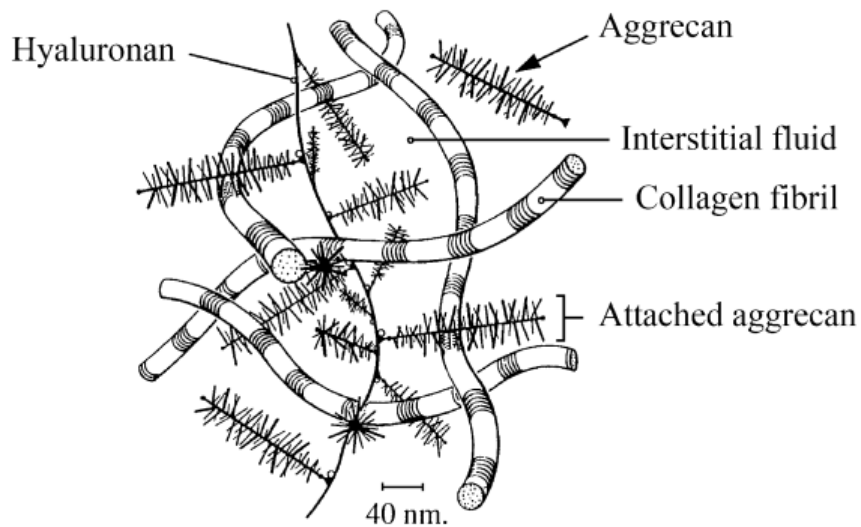


Figure 2.1 Schematic representation of the collagen network interacting with the proteoglycan network, forming a porous solid matrix in articular cartilage. From Lu [29], with permission.

To investigate the mechanical behaviors of cartilage under compression, three types of mechanical testings are generally adopted: unconfined compression [20, 21, 23, 31-33], confined compression [7, 34] and indentation [1, 3, 22, 28, 35-37]. Compared with the other two, indentation testing has a few advantages. It is site specific, non-destructive, and suitable for testing on small joints when limited amount of tissue is available. A schematic configuration of indentation testing is shown in Fig. 2.2. Since indentation problem has complicated boundary conditions, the analysis is not as straight forward as the other two methods. One of the earliest attempts to analyze the cartilage indentation problem was done by Sokoloff et al. [38], using the method developed by Hertzian studying non-adhesive elastic contact. By assuming the cartilage being linear elastic incompressible infinite half space and the cylindrical indenter tip being rigid, the elastic modulus of cartilage can be calculated by the equation

$$E = \frac{F}{2.67Rd}. \quad (2.1)$$

Here, F is the reaction force on the indenter, R is the radius of the indenter, and d is the indentation depth.

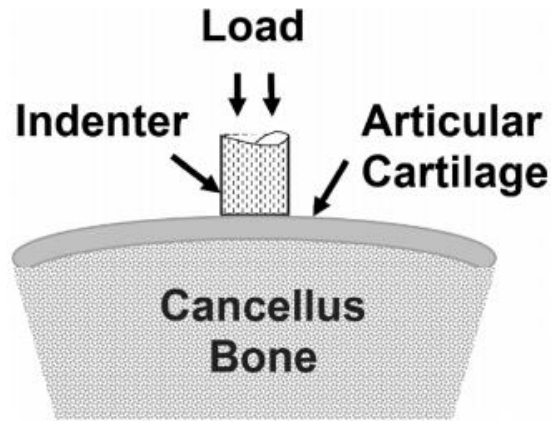


Figure 2.2 A schematic diagram of indentation test. From Lu [29], with permission.

Since the articular cartilage thickness is often at the same scale of the indenter size, the infinite half-space assumption is in fact inappropriate and the Hertzian method overestimates the tissue stiffness. In the 1970s, Hayes et al. [1] developed the solution for indentation on a layered linear elastic material. The Young's modulus of the material is given by

$$E = \frac{F(1-\nu)(1+\nu)}{2Rd\kappa\left(\frac{R}{h}, \nu\right)}. \quad (2.2)$$

Here, h , is the thickness of the cartilage, and κ , is an integration function associated with the shape of the indenter tip. To determine the Young's modulus, reaction force, F , indentation depth, d , indenter radius R , cartilage thickness, h , and Poisson's ratio, ν , are needed.

When the tissue is subject to compressive loading, a volumetric change could be induced within the tissue. As each component of the tissue, i.e. collagen, proteoglycan, water, can be assumed incompressible [7], the volumetric change results in the interstitial water being extruded from the tissue. Since the gaps between

collagen fibers are only hundreds of nano meters, the relative motion between the interstitial water and collagen matrix generates very high frictional drag forces, giving rise to the flow-dependent viscoelastic behavior of the cartilage. Due to this viscosity, the tissue could take a long time to reach equilibrium, e.g., 1 to 3 hours for indentation on adult bovine knee cartilage [3]. By far, the most successful theory to describe the flow-dependent behaviors of cartilage is the biphasic theory [7], which assumes the tissue to be a binary mixture of water and elastic solid. To characterize the time dependent response, an additional mechanical property, permeability, is adopted in this theory. Analytical solution of indentation on biphasic linear elastic (BLE) material is given in [8] and a numerical curve-fitting method [9] is developed to determine the Young's modulus, Poisson's ratio, and permeability from a single indentation creep curve, as shown in the right of Fig. 2.3 .

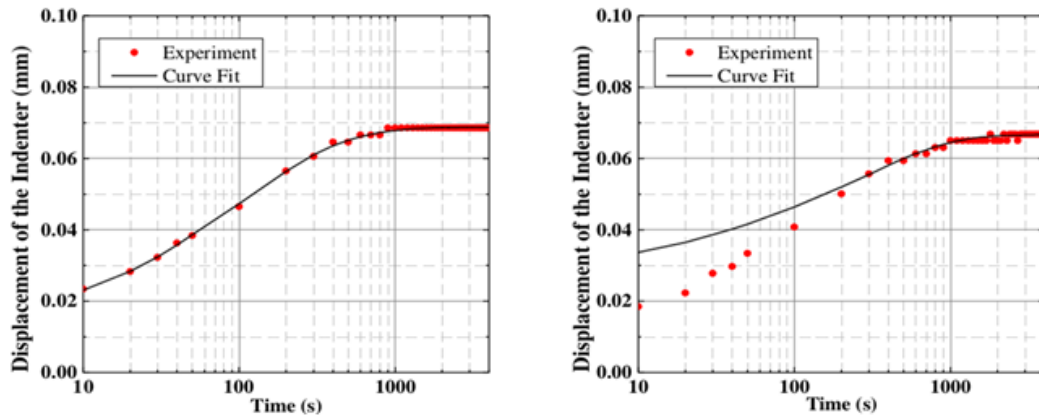


Figure 2.3 An indentation creep curve fitted by nonlinear (left) and linear (right) elastic biphasic models

Cartilage is experimentally shown to have one order of magnitude difference in terms of the modulus under compression and tension. This difference has significant impact on the response of the cartilage under indentation. For example, at the very beginning of the creep test, according to the biphasic theory, the material is almost incompressible. Thus, the tensile modulus in lateral directions can directly contribute to the stiffness in the loading direction. By setting a higher modulus in tension, the difference between the BLE model and experiments can be reduced, as shown in Fig. 2.3. Many models are available to catch this nonlinearity in tension and compression in cartilage. Among them, the CLE model and continuous fiber distribution (CFD) model are commonly used [21, 39]. In addition to the properties identified in the BLE model, a new material property, tensile modulus, is introduced for the solid matrix. In BLE model, the tensile and compressive moduli are the same. Due to the complexity of the nonlinear constitutive models, an analytical solution for indentation is difficult to obtain. Thus, the finite element (FE) method and curve-fitting are generally adopted to extract mechanical properties for the newly developed models.

Chapter 3

USING PRINCIPAL COMPONENT ANALYSIS TO SHORTEN THE INDENTATION TESTING TIME

3.1 Introduction

The lengthy time required for the indentation testing of cartilage tissue not only reduces the efficiency of indentation and hinders *in vivo* applications, but also could possibly lead to tissue degeneration during the testing. In this chapter, a data processing technique is developed to predict the full indentation creep curve based on the transient data obtained in the first few minutes of indentation testing. The accuracy of the prediction is verified using experimental data from two types of articular cartilage - bovine knee cartilage and condylar cartilage from the porcine TMJ. The mechanical properties determined by biphasic theory, based on the predicted curves, are compared with those from full experimental data in order to validate the accuracy of this method.

3.2 Method

3.2.1 Experiments

Indentation creep tests were performed on condylar cartilage from porcine TMJ and bovine knee joint cartilage, as described in previous studies [3, 28]. Briefly, seventeen 2 cm x 2 cm rectangular cartilage bone blocks were harvested from the trochlear groove of mature bovine knee joints. Samples were mounted onto a step-loading indentation device equipped with a rigid flat-ended porous-permeable indenter tip ($\phi = 2.1$ mm). At the start of the creep test, a 50 mN tare load was applied for 0.5 h, followed by a 200 mN step load for another 1 h to generate the creep data.

Additionally, eight TMJs, were harvested from mature porcine heads, and five regions (anterior, posterior, central, and lateral) on the condylar head were indented by a custom built micro-indenter with a porous-permeable indenter tip ($\phi = 1.6\text{mm}$); using the same loading protocol detailed for bovine cartilage [28].

3.2.2 Principal component analysis

The creep displacement of each sample was first resampled at 1 Hz by linear interpolation and denoted as an $n \times 1$ vector t . Vectors from m samples were further combined into an $m \times n$ matrix. PCA [40] was then conducted on this matrix without centering, which generated m principal components. Each principal component is an $n \times 1$ unit vector, denoted as PC_i . Based on the PCA definition, the creep curve (vector t) can be decomposed by the principal component matrix PC as.

$$\begin{bmatrix} t_1 \\ t_2 \\ \vdots \\ t_n \end{bmatrix} = \begin{bmatrix} PC_{1_1} & PC_{2_1} & \cdots & PC_{m_1} \\ PC_{1_2} & PC_{2_2} & \cdots & PC_{m_2} \\ \vdots & \vdots & \ddots & \vdots \\ PC_{1_n} & PC_{2_n} & \cdots & PC_{m_n} \end{bmatrix} \begin{bmatrix} c_1 \\ c_2 \\ \vdots \\ c_m \end{bmatrix} \quad (3.1)$$

$$\text{or } t^T = \sum_{i=1}^m c_i * PC_i^T \text{ where } c_i = t \cdot PC_i. \quad (3.2)$$

Here vector c includes coefficients with the same units as vector t . We now hypothesize that the principal components are consistent for the same type of cartilage tested with an identical protocol. Therefore the creep curves of the other samples, which are not initially included in the m samples for PCA, can also be decomposed by the above principal components PC . To verify this assumption, we performed PCA on 50 different combinations of 5 indentation creep curves that were randomly selected from either bovine knee joint samples or TMJ samples, *i.e.* 50 PCA for each type of cartilage. The variances of 50 obtained PCs at each time point (n total points) were calculated to determine the consistency of PCs .

Based on the PCA consistency assumption, the short-term creep displacement \hat{t} of a new sample can be decomposed by the principal component matrix PC as

$$\begin{bmatrix} \hat{t}_1 \\ \hat{t}_2 \\ \vdots \\ \hat{t}_k \end{bmatrix} \approx \begin{bmatrix} PC_{1_1} & PC_{2_1} & \dots & PC_{m_1} \\ PC_{1_2} & PC_{2_2} & & PC_{m_2} \\ \vdots & \vdots & \ddots & \vdots \\ PC_{1_k} & PC_{2_k} & \dots & PC_{m_k} \end{bmatrix} \begin{bmatrix} \hat{c}_1 \\ \hat{c}_2 \\ \vdots \\ \hat{c}_m \end{bmatrix} \quad (3.3)$$

$$\text{or } \hat{t}(1:k)^T = \sum_{i=1}^m \hat{c}_i * PC_i(1:k)^T, k < n. \quad (3.4)$$

Here vector $\hat{t}(1:k)$ contains only k components ($k \ll n$) since it represents only the first k seconds of a creep curve. $PC_i(1:k)$ denotes the first k components of PC_i . If the shortened principal component matrix is denoted as B , the coefficient vector \hat{c} can be calculated as

$$\hat{c} = (B^T B)^{-1} B^T \hat{t}(1:k)^T. \quad (3.5)$$

Note that \hat{c} is the coefficient vector with m components. The long term creep deformation of the sample after k seconds $\hat{t}(k+1:n)$, can be estimated using \hat{c} and matrix PC .

$$\begin{bmatrix} \hat{t}_{k+1} \\ \hat{t}_{k+2} \\ \vdots \\ \hat{t}_n \end{bmatrix} \approx \begin{bmatrix} PC_{1_{k+1}} & PC_{2_{k+1}} & \dots & PC_{m_{k+1}} \\ PC_{1_{k+2}} & PC_{2_{k+2}} & & PC_{m_{k+2}} \\ \vdots & \vdots & \ddots & \vdots \\ PC_{1_n} & PC_{2_n} & \dots & PC_{m_n} \end{bmatrix} \begin{bmatrix} \hat{c}_1 \\ \hat{c}_2 \\ \vdots \\ \hat{c}_m \end{bmatrix} \quad (3.6)$$

$$\text{or } \hat{t}^T(k+1:n) = \sum_{i=1}^m \hat{c}_i * PC_i^T(k+1:n). \quad (3.7)$$

Thus PCA of the full creep curves from a small group of samples can generate the principal component matrix, and then the long-term creep data of the other samples can be predicted by their short term response using this matrix.

3.2.3 Accuracy of predicted data

To test the accuracy of the predicted curve, eight sets of full indentation data were randomly selected for each type of cartilage to generate the corresponding

principal components, and the first 10 minutes of data from the unselected samples were used to predict their long-term response with PCA. The predicted curves were directly compared with the actual long-term experimental data. Moreover, the mechanical properties (aggregate modulus, Poisson's ratio, permeability) were obtained for both the predicted curve and the actual experimental data using a biphasic curve-fitting program [9]. The agreement between the two sets of mechanical properties was then examined [41].

3.3 Results

To understand the effectiveness of PCA for predicting cartilage indentation data, PCA of all the creep curves was performed to obtain the contribution to the total variance of each principal component (Fig. 3.1). The first *PC* alone contributes 98.5% and 99.8% to the total variance for TMJ and knee cartilage, respectively. The first and second *PCs* contribute over 99.5% of the variance for both tissues. Thus, in the following *PC* consistency analysis, only the first two *PCs* were presented, as the third and higher *PCs* contribute little to the total variance. For each type of tissue, average and standard deviation of the first two *PCs* from 50 analyzed groups are shown in Fig. 3.2. The standard deviations are close to 0 for *PC1* at all points, *i.e.*, *PC1* remains constant for any five randomly selected indentation curves. The standard deviations of *PC2* are larger than *PC1*, but *PC2* accounts for only 1.4% and 0.1% of variance for TMJ and knee cartilages, respectively. Therefore, it can be concluded that the principal components are consistent for the same type of cartilage. In contrast to this, indentation curves of TMJ and knee cartilage have drastically different *PCs* in terms of magnitude and distribution over time (Fig. 3.2).

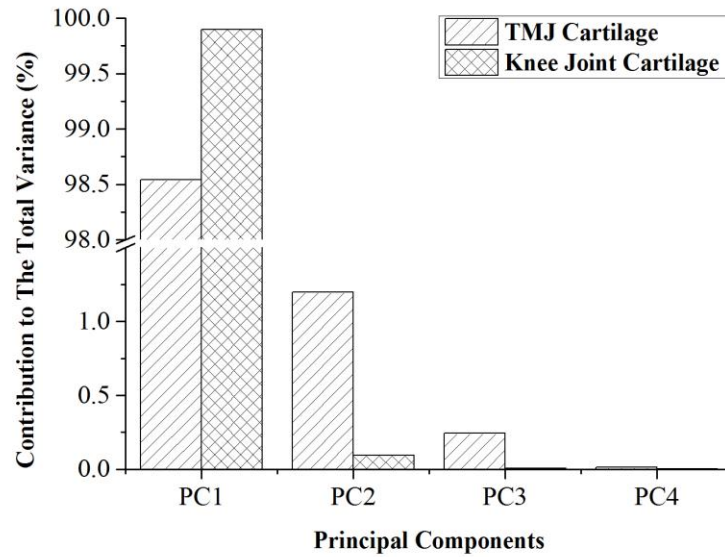


Figure 3.1 Contribution of principal components to the total variance of indentation creep curves. The first principal component (*PC1*) explains 98.5% and 99.8% of the total variance for TMJ cartilage and knee joint cartilage, respectively. The third principal component contributes less than 0.5%.

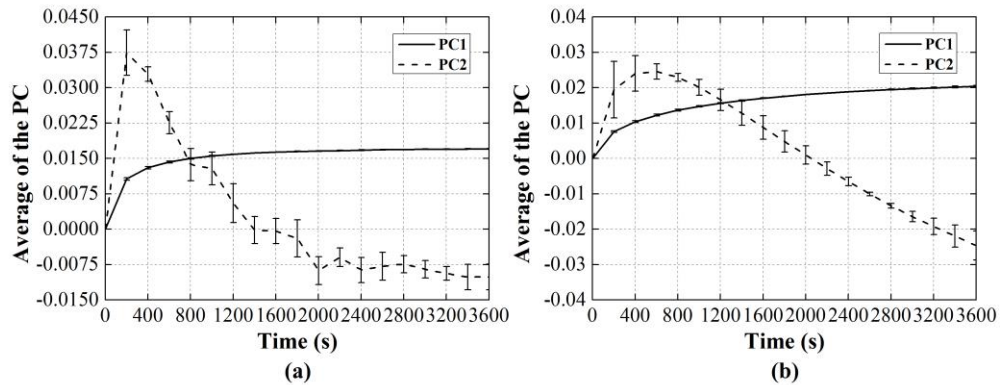


Figure 3.2 Average principal components of 50 random combinations of 5 indentation creep curves for (a) TMJ condylar cartilage and (b) knee joint cartilage. The first principal component (*PC1*) of any five creep curves remains highly consistent with low standard deviations at all time. The second principal component (*PC2*) is not as consistent as *PC1*.

Two typical experimental creep curves for each cartilage are plotted in Fig. 3.3 together with the PCA prediction. The first 10 minutes of data and the *PCs* based on eight creep curves are able to provide an accurate prediction of the long-term indentation responses for both types of cartilage. The average difference of equilibrium deformation between experiment and PCA is $4.5 \pm 1.1\%$ for bovine knee cartilage and $5.1 \pm 1.3\%$ for porcine TMJ cartilage. This difference was also determined for varying numbers of creep curves used to obtain the *PCs* (Fig. 3.4). For both types of cartilage, *PCs* from 11 or more creep curves generate similar prediction errors.

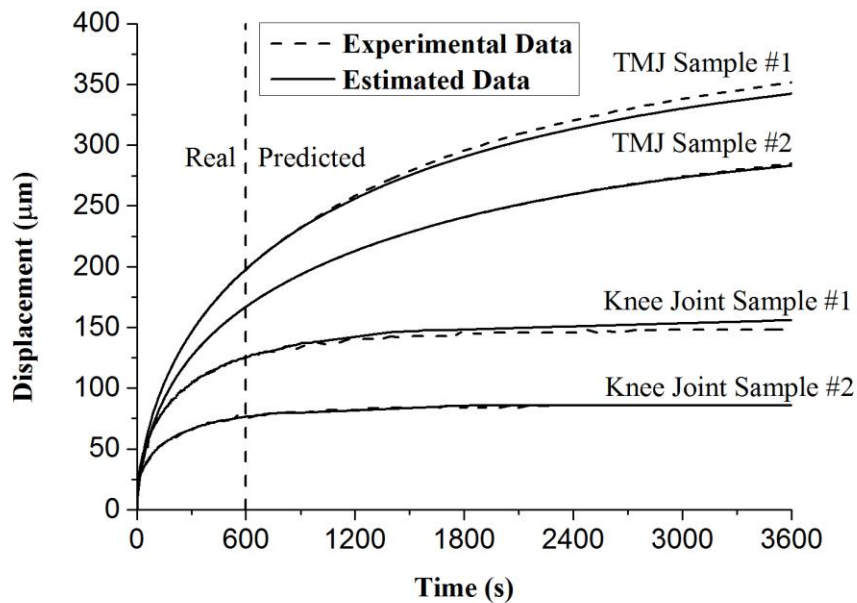


Figure 3.3 PCA predicted indentation creep curves of two samples for each type of cartilage, using the experimental data in the first 600 seconds. The corresponding full experimental curves are also plotted for comparison.

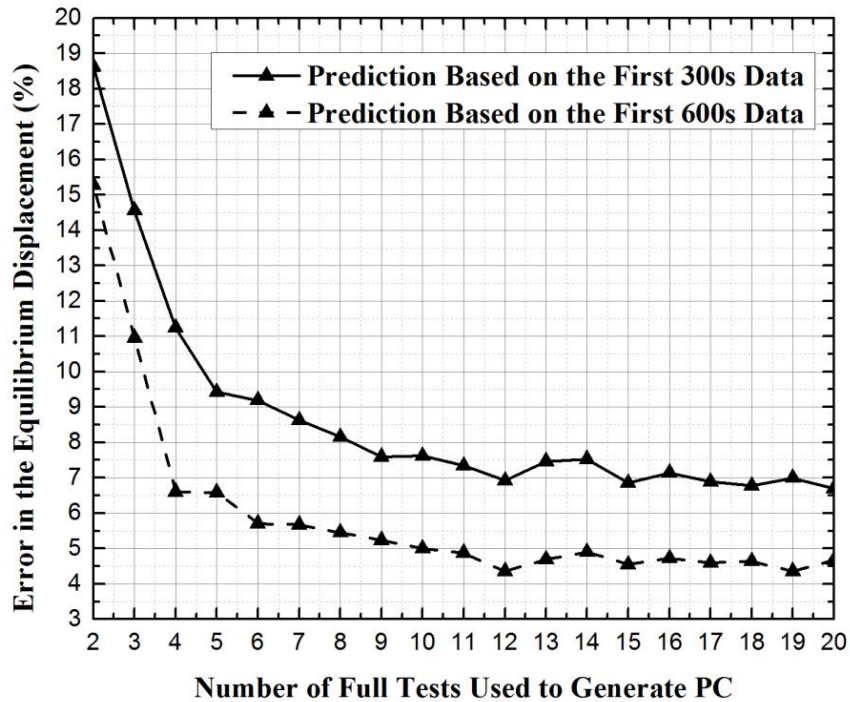


Figure 3.4 The PCA prediction errors are correlated with the number of full tests used for *PC* matrix construction and the length of initial testing data available for prediction.

The mechanical properties determined by biphasic curve-fitting based on the experimental and predicted data are summarized in Fig. 3.5. The magnitudes of all properties are consistent with those reported in the literature [3, 28, 42]. The data points are clustered around the line $Y=X$ in each plot, and the coefficient of determination is close to 1 for all three mechanical properties, displaying excellent agreement between both data sets. The errors (mean \pm standard deviation) of the estimated mechanical properties of TMJ condylar cartilage are $3.3 \pm 3.3\%$, $2.0 \pm 2.0\%$ and $3.2 \pm 3.2\%$ for aggregate modulus, permeability and shear modulus, respectively. For bovine knee joint cartilage the corresponding errors are $2.2 \pm 3.1\%$, $7.4 \pm 12.4\%$

and $3.1 \pm 4.3\%$, respectively. The mean difference of the aggregate moduli is close to zero, and the 95% confidence interval of the differences (mean $\pm 2 \times$ SD) is less than 20% of the average (Fig. 3.6), showing excellent agreement between the two data sets. In addition, the differences show no dependency on the magnitude of the aggregate modulus [41].

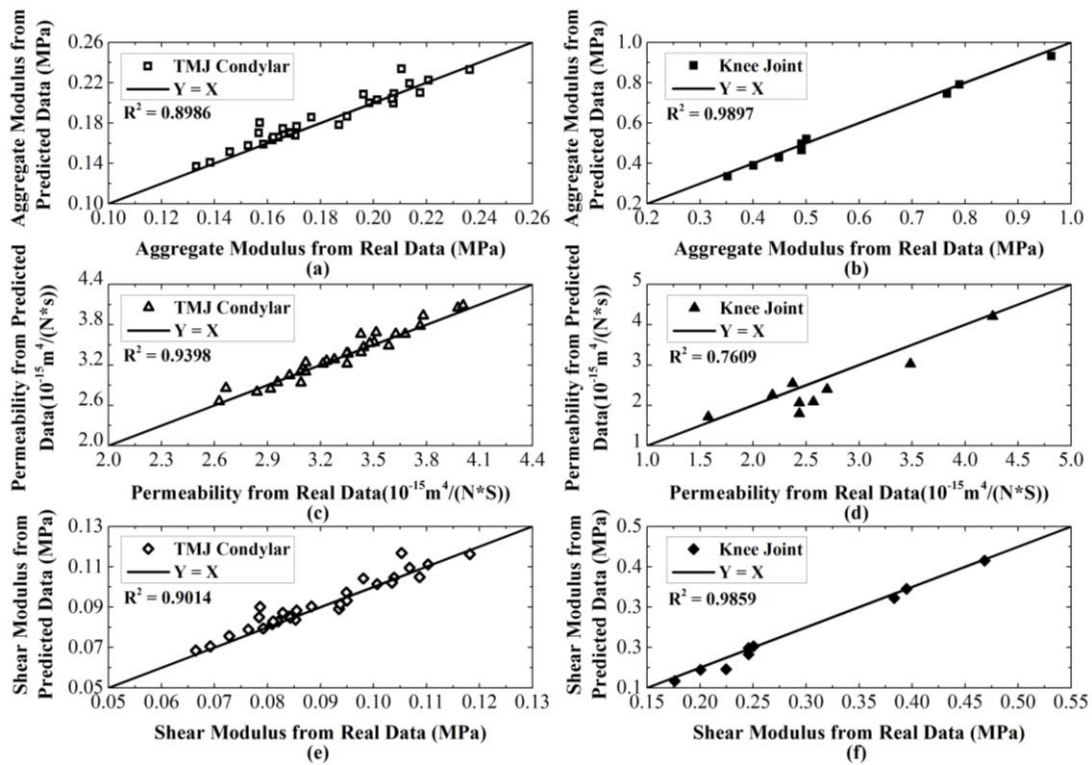


Figure 3.5 Comparison of mechanical properties determined by indentation curve-fitting using experimental and PCA predicted curves, (a-b) aggregate modulus, (c-d) permeability, and (e-f) shear modulus. Line $Y=X$ is plotted for reference.

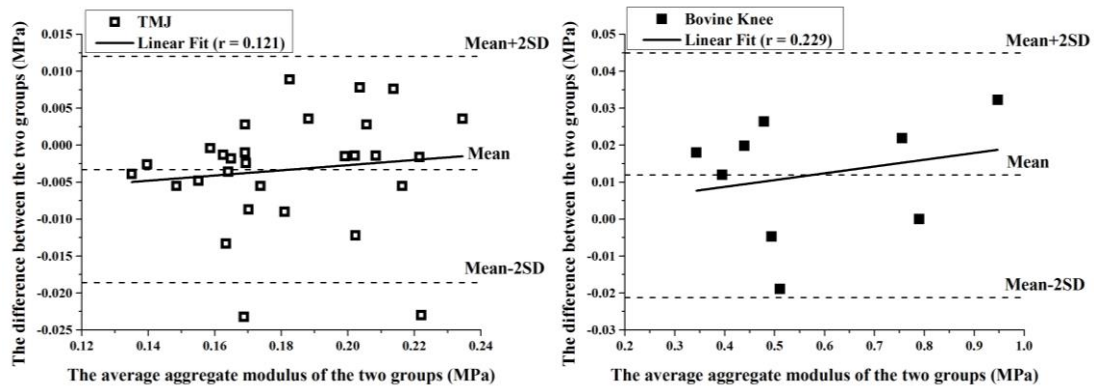


Figure 3.6 The difference of aggregate modulus determined from predicted and experimental data is plotted against their average value. For most samples, the difference is smaller than 5% of the average value, and the mean of the difference is close to zero (-0.003Mpa for TMJ and 0.012Mpa for knee). In addition, the difference between two data sets is not dependent on their average values. All these factors indicate that the two data sets have a good agreement.

3.4 Discussion

PCA, for the first time, is employed to analyze cartilage indentation creep curves for two types of cartilage with different ultrastructure and mechanical properties [28, 43]. The creep deformation of cartilage under indentation can be accurately decomposed by *PCs*, and the first two *PCs* contribute over 99.5% of the variance. More importantly, the *PCs* are consistent for the same type of cartilage tested with identical protocols, which provides the theoretical foundation to predict the full deformation curve using PCA based on the transient data of the first few minutes. As expected, the predicted creep curves match the actual experimental data well, and the mechanical properties determined from the two sets of curves agree with each other.

Unlike hyaline cartilage in knee joints, the TMJ condylar cartilage is a fibrocartilaginous tissue with a unique dense fibrous zone composed of large type I collagen bundles covering the articular surface [44]. *PCs* of the creep curves from these two distinct cartilages are completely different. This implies that PCA could be a powerful method to compare the mechanical behaviors of different cartilages. In this study, *PCs* from 100 combinations of 5 samples were consistent. Comparison of the first PC alone can reveal significant differences between the mechanical properties of healthy and degenerated cartilages (Fig. B.4).

Adding more *PCs* or full tests can be helpful at low sample numbers. Meanwhile, for both knee cartilage and TMJ condyle in our experiments, any number of full tests beyond eight will not lead to an increase higher than 1% in the accuracy (Fig. 3.4). In addition, the average error increases 2% when only 300 seconds' data is used for prediction instead of 600 seconds, and this gap cannot be reduced by increasing the number of full tests used to generate the *PC*.

Chapter 4

DETERMINING THE TENSION-COMPRESSION NONLINEAR MECHANICAL PROPERTIES WITH FINITE ELEMENT ANALYSIS

4.1 Introduction

In this chapter, we aimed to develop a technique to uniquely determine the nonlinear biphasic properties of cartilage from a single indentation creep test. First, the roles of permeability, tensile and compressive moduli in the indentation response of cartilage were analyzed and identified. Second, an optimization algorithm was designed based on these findings, which can simultaneously and uniquely determine the three properties by fitting a single indentation curve. Third, the new algorithm was applied to analyze the experimental data from adult bovine knee cartilage, and the results were validated by comparison with the classical biphasic linear elastic program.

4.2 Method

4.2.1 Experiment

Seventeen cartilage bone blocks, without removing the superficial layer, were harvested from the trochlear groove of two skeletally mature (18 months old) bovine knee joints, in a region where the articular surface has relatively small curvature. Indentation testing was performed as described previously [3]. In brief, samples were submerged in PBS supplemented with protease inhibitors and tested on an indentation device equipped with a rigid, porous, flat-ended cylindrical indenter tip ($\phi = 2.1$ mm). A 50 mN tare load was first applied for 0.5 h to ensure full contact between the indenter and cartilage surface. Then a 200 mN step load was applied and maintained

for another 1 h or until the creep deformation reached equilibrium. The cartilage thickness at the testing spot was later measured using the needle penetration method [9].

4.2.2 Nonlinear constitutive models

In the numerical simulations, the cartilage is modeled as a biphasic material with a tension-compression nonlinear solid matrix, which is treated as a compressible isotropic neo-Hookean ground matrix reinforced with fibers. The fibers can only sustain tensile stress, therefore the compressive modulus of the material is defined to be the Young's modulus of the neo-Hookean background at small strain [22]. When the fibers are organized in three orthogonal directions, this constitutive model displays mechanical behaviors similar to a CLE material with cubic symmetry and henceforth is referred to as the CLE model. Based on earlier experimental results [18], the strain energy density function of the fiber bundles is defined as [39]

$$\Psi = \frac{\xi}{\alpha\beta} \left(e^{\alpha(I_n-1)^\beta} - 1 \right) \quad (4.1)$$

and the Cauchy stress of the fiber is given by

$$\boldsymbol{\sigma} = H(I_n - 1) \frac{2I_n}{J} \frac{\partial \Psi}{\partial I_n} \mathbf{n} \otimes \mathbf{n} \quad (4.2)$$

$$I_n = \lambda_n^2 = \mathbf{N} \cdot \mathbf{C} \cdot \mathbf{N} \text{ and } \mathbf{n} = \frac{\mathbf{F} \cdot \mathbf{N}}{\lambda_n^2}. \quad (4.3)$$

In these equations, \mathbf{N} is the unit vector in the fiber direction, \mathbf{C} is the right Cauchy-Green deformation tensor, λ_n is the stretch ratio, \mathbf{F} is the deformation gradient, J is the Jacobian of the deformation, and H is a Heaviside function used to ensure zero resistance of the fibers under compression. The parameter ξ is nonlinearly correlated with the fiber stiffness, and is referred to as the fiber modulus in this model. Constants α and β are set to 0 and 2 to render an almost linear stress-strain relationship at small

strains [39], in which case the tissue tensile modulus E_f in the fiber direction can be written as

$$E_f \approx 4\xi \quad (4.4)$$

Alternatively, a number of studies assume the fibers are continuously distributed, as known as a CFD model. In this case, the strain energy density function of the fibers is still given by Eq. 4.2, while the Cauchy stress is integrated over all possible fiber directions [39].

$$\boldsymbol{\sigma} = \iint H(I_n - 1) \boldsymbol{\sigma}_n(\mathbf{n}) \sin\varphi d\varphi d\theta \quad (4.5)$$

$$\boldsymbol{\sigma}_n(\mathbf{n}) = \frac{2I_n}{J} \frac{\partial \Psi}{\partial I_n} \mathbf{n} \otimes \mathbf{n} \quad (4.6)$$

Here, φ and θ are the spherical angles of the fiber orientation in the local coordinate system [45].

In this study, the hydraulic permeability of the cartilage is assumed to be constant, homogeneous, and isotropic. Poisson's ratio of the neo-Hookean ground matrix is assumed to be 0 as suggested in the literature [18, 21]. Two 3D FE models for the indentation creep test were built in FEBio 2.0 [45], based on the biphasic CLE and CFD models respectively. Taking advantage of the axisymmetric nature of the indentation test, a 1° wedge of the cartilage and indenter (modeled as rigid) was analyzed with symmetry boundary conditions applied on the circumferential faces. The other boundary conditions are defined to be consistent with the actual experimental conditions (Fig. 4.1). The FE mesh was biased in order to capture the rapid variation of the strain field and fluid pressure near the cartilage indenter interface. A mesh convergence study was performed and the resulting mesh contained 2627 nodes and 1250 elements, including 1225 HEX8 type and 25 PENTA6 type elements. In the FE simulation, a constant force is applied on the indenter as a

Heaviside function, and the displacement of indenter tip is calculated to generate the creep deformation curve. The results of the FE program serve as the basis for the curve-fitting technique to determine the mechanical properties from the indentation experiments.

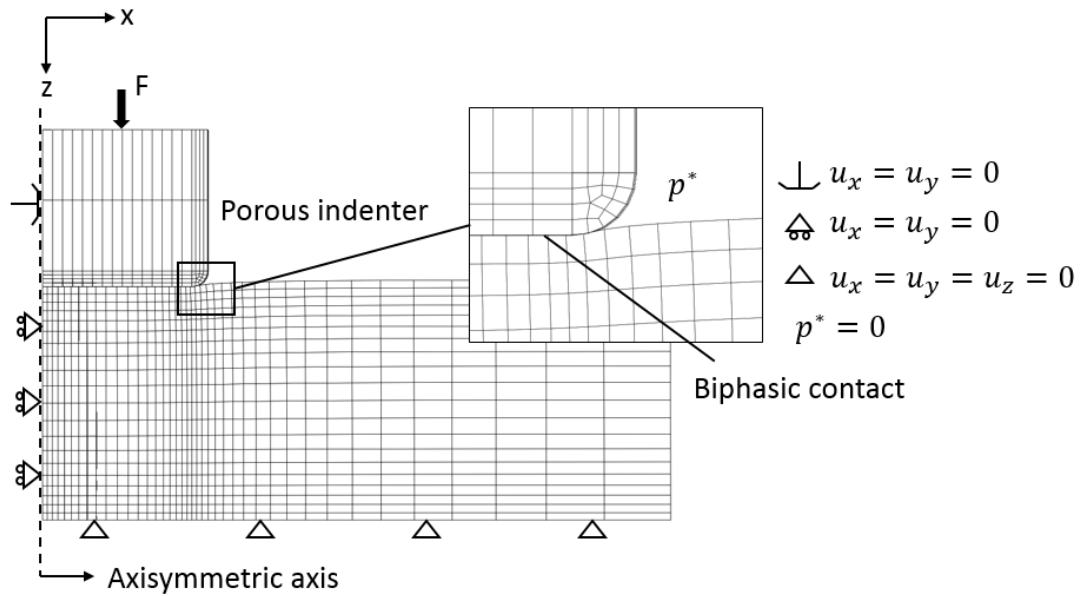


Figure 4.1 A one-degree wedge of cartilage and indenter is meshed and analyzed based on the axial symmetric nature of indentation tests. The bottom of the cartilage is impermeable and fixed in all directions to mimic the cartilage-bone interface. Deformation of the contact surface is associated with the movement of the indenter tip, and the fluid pressure is set to be zero (porous indenter). u_x , u_y , and u_z represent the displacement in x , y , and z directions, respectively, and P is the fluid pressure.

4.2.3 Optimization algorithm

As an initial step toward developing the curve-fitting algorithm, the FE models were used to perform parametric studies to identify the effect of individual mechanical properties on the indentation creep deformation. Each of the three key parameters

(compressive modulus E , permeability k , and fiber modulus ζ) was varied within the physiological range while keeping the other two constant. Results based on the biphasic CLE model are plotted over time on a logarithmic scale in Fig. 4.3. The CFD model displayed the same trends (results not shown). The compressive modulus E has a significant effect on the equilibrium deformation (Fig. 4.3a), while the fiber modulus mainly regulates the transient deformation in the early portion of the curve (Fig. 4.3c). Varying the permeability does not change the overall slope of the curve or the equilibrium deformation, but shifts the deformation curve along the time axis (Fig. 4.3b).

In light of these observations, three defining characteristics of the creep curve are identified (Fig. 4.2a): the equilibrium deformation μ , the deformation ratio γ , and the half deformation time τ . Equilibrium deformation μ is the deformation at steady state. The deformation ratio γ represents the ratio between the initial jump and equilibrium deformation, where the initial jump equals the indenter displacement at 5 s after the onset of loading. Half deformation time τ is the time at which the deformation reaches the halfway point between the initial jump and equilibrium deformation, and is an indication of the viscoelastic relaxation time of the tissue. The correlations between these parameters (*i.e.*, μ , γ , and τ) and the mechanical properties (*i.e.*, E , k , and ζ) were plotted in Fig 4.3d-f. Both the fiber modulus and compressive modulus are negatively correlated with the tissue equilibrium deformation, and they have opposite effects on the deformation ratio (Fig. 4.3d, f). The permeability is positively correlated with the deformation ratio and negatively correlated with the half deformation time (Fig. 4.3e).

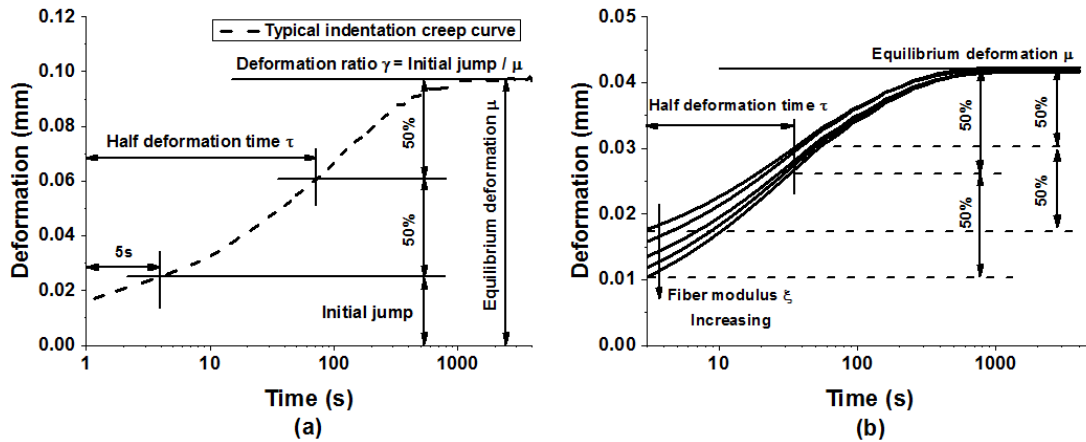


Figure 4.2 (a) A typical indentation creep curve from tests on bovine knee cartilage and the definition of three curve-related parameters, including the initial jump, equilibrium deformation, and half deformation time. (b) When the equilibrium deformation and half-deformation time are fixed, the initial jump of the curve is regulated by the fiber modulus.

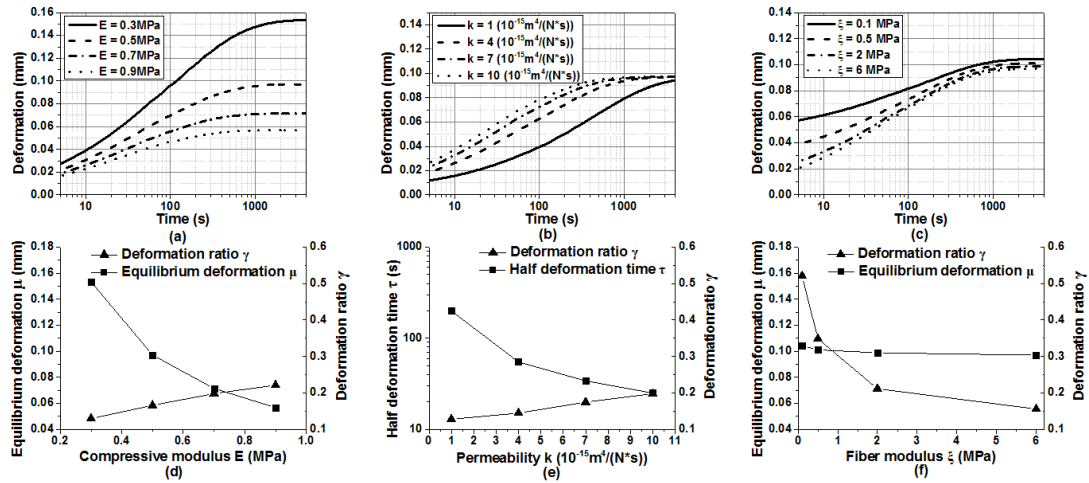


Figure 4.3 Roles of each individual mechanical property in shaping the indentation creep curve in biphasic CLE model. Creep curves are plotted by varying one of the three properties in the physiological range and keeping the other two constant (compressive modulus = 2MPa, fiber modulus = 2MPa, permeability = $0.001 \text{ mm}^4 \cdot \text{N}^{-1} \cdot \text{s}^{-1}$): (a) compressive modulus, (b) permeability, and (c) fiber modulus. (d-f) Monotonic correlations between the mechanical properties and the deformation ratio, half deformation time, and equilibrium deformation are observed.

In order to determine the individual mechanical properties (E , k , and ζ) from a single indentation experiment, the FE prediction is curve-fitted to the experimental creep curve. First, a fiber modulus ζ at the middle of the search range, which is set to be 0 ~ 5MPa for the CLE model, and 0 ~ 2 MPa for the CFD model based on previous studies [21, 39, 46], is selected as the starting value. The equilibrium deformation μ is a function of both the compressive modulus, E , and fiber modulus, ζ , but not the permeability, k . When ζ is fixed, μ decreases monotonically with increasing E (Fig. 4.3d),

$$\left(\frac{\partial\mu}{\partial E}\right)_{\zeta} < 0. \quad (4.7)$$

Therefore, a value for E corresponding to the assumed ζ can quickly be determined using a binary search based on μ . Next, a similar process is used to find the appropriate value of k corresponding to the assumed value of ζ . According to Fig 4.3e, an increase in the permeability, k , shifts the creep curve to the left with no effect on the equilibrium deformation,

$$\left(\frac{\partial\tau}{\partial k}\right)_{E,\zeta} < 0. \quad (4.8)$$

Thus k can also be determined using a binary search based on the half deformation time, τ .

What remains is to check the accuracy of the assumed magnitude of ζ , which can be done by considering the remaining parameter of the creep curve, the deformation ratio, γ . With fixed values of E and k , variations in ζ significantly change the initial jump (Fig. 4.3c), which in turn affects the deformation ratio, γ . When μ and τ are fixed, ζ is found to be monotonically related to the deformation ratio, γ (Fig.

4.2b). Thus another binary search can be used to find the value of ζ corresponding the experimentally determined μ and τ ,

$$\left(\frac{\partial \gamma}{\partial \xi}\right)_{\tau, \mu} < 0. \quad (4.9)$$

This updated value of ζ is then used as the new starting value, and the entire process is repeated. The overall curve-fitting strategy is a two-level, embedded binary search as illustrated in Fig. 4.4. At the lower level, the compressive modulus and permeability are searched sequentially to match the equilibrium deformation and half deformation time for an assumed fiber modulus, ζ . At the higher level, ζ is optimized to match the deformation ratio of the creep curve. Since the calculation of the equilibrium deformation is merely a static mechanics problem with no time dependent integration, the computational cost of this step is negligible. Moreover, all three parameters are determined using a binary search algorithm. The running time of the algorithm is $O(\log^2 n)$, where n is the number of partitions in the search range. Therefore, the optimization strategy runs efficiently and avoids the possible optimization complications of multiple solutions and local minima.

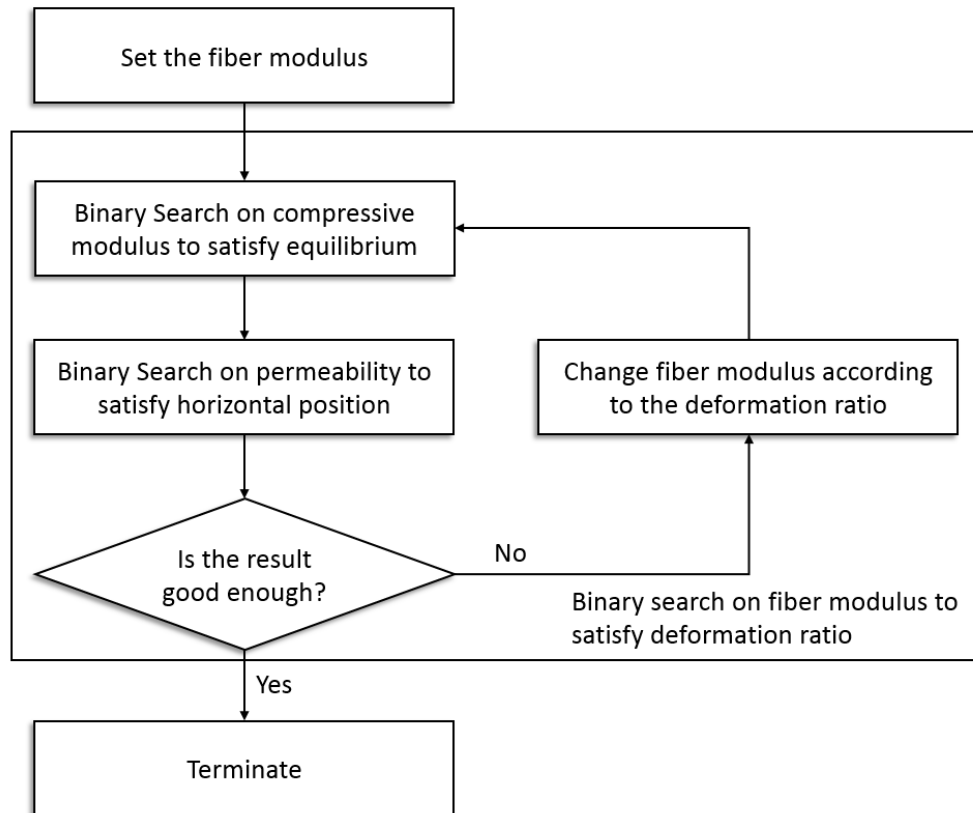


Figure 4.4 The optimization scheme involves two levels of binary search. At the lower level, given a fiber modulus, the compressive modulus and permeability are optimized to fit the equilibrium deformation and half deformation time of the curve. At the higher level, the fiber modulus is searched to match the deformation ratio. Adjustment of fiber modulus requires a new search of compressive modulus and permeability.

The optimization program is implemented in MATLAB 2013a (The MathWorks Inc.), where indentation creep simulations are handled by calling the FEBio program for each iteration. The error tolerance in the optimization was chosen at 0.5%. The creep data from the indentation tests on bovine cartilage have been analyzed using both the CLE and CFD models, and the accuracy of the fit is measured by

$$R^2 = 1 - \frac{\sum(f_i - y_i)^2}{\sum(y_i - \bar{y})^2}, \quad (4.10)$$

where f_i and y_i are the i^{th} simulation and i^{th} experimental data point, respectively, and \bar{y} is the mean of y . The corresponding mechanical properties in the CLE and CFD models are correlated using a linear regression test, and they were also compared with those given by the classic curve-fitting program based on the BLE model [9, 42]. The aggregate moduli, which is defined as the modulus under confined compression, and permeability from the three models were compared by one-way ANOVA with Tukey's post hoc test ($p < 0.05$) on repeated measures.

4.3 Results

Two typical experimental indentation creep curves fitted by the optimization technique using both biphasic CLE and CFD models, as well as the classical BLE curve fitting program, are shown in Fig. 4.5a. The CLE and CFD models generate nearly overlapping curves that match the experiments well over the entire time domain. The BLE fits the equilibrium deformation accurately, but not the short-term transient response since it is based on the elastic Hayes solution. In the actual experiment, immediately after the step loading, the cartilage behaves like an incompressible material, due to the interstitial fluid pressurization [23]. Thus the compressive deformation in the loading direction has to be associated with tissue expansion in the radial direction. However, the relatively high tensile stiffness of the tissue provides resistance to this radial expansion, which in turn constrains the initial axial deformation. The high tensile stiffness featured in the CLE and CFD models allows these models to capture this short-term response and significantly improves the curve-fitting accuracy by reducing the initial jump. The average R-squared value of the fitted curves is 0.988 ± 0.014 for the CLE model, 0.988 ± 0.013 for the CFD model,

and 0.781 ± 0.082 for the BLE model. To determine the three mechanical properties using an experimental creep curve, ~ 600 seconds computing time is required on a personal computer (Intel i5 3rd generation processor, 4 cores @ 3.4 GHz, and 16 GB memory). A typical optimization process is plotted in Fig 4.5b, which shows that four iterations may be enough to obtain a satisfactory fit to the fiber modulus ζ .

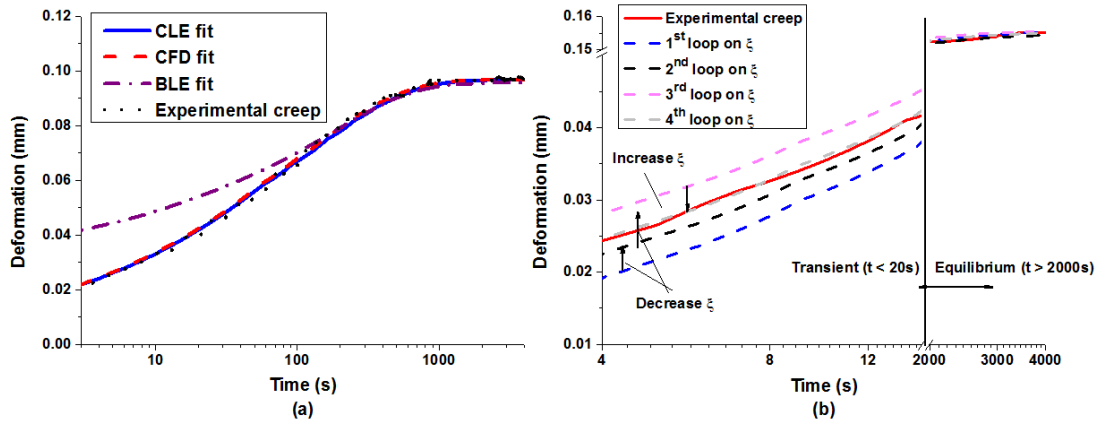


Figure 4.5 (a) Typical indentation creep displacement history of adult bovine knee cartilage and the curve-fittings based on BLE and biphasic CLE and CFD models. (b) Typical searching process for fiber modulus ζ . The dashed lines are simulated curves over different ζ values after fixing equilibrium deformation and half deformation time.

The mechanical properties determined from the curve-fits using the three different constitutive models are listed in Table 3.1. The aggregate moduli were 0.438 ± 0.253 MPa, 0.415 ± 0.248 MPa, and 0.451 ± 0.228 MPa for the CLE, CFD, and BLE models, respectively. One-way ANOVA shows that all three models differ from each other and the BLE model generates the highest compressive modulus, which is expected as the BLE model lumps the effect of the high tensile stiffness into the

aggregate modulus and therefore increases the calculated value of the compressive modulus. The compressive moduli from the two nonlinear models are linearly correlated with each other, with a correlation coefficient R of 0.99 (Fig 4.6a). The slope of the linear fit is 1.02, and the offset is 0.01 MPa. The aggregate moduli from both nonlinear models are highly correlated with those from the BLE model ($r > 0.99$) (Fig. 4.7a).

Table 3.1 Mechanical properties determined by BLE, CLE, and CFD models (*: different from CFD; +: different from CLE).

	CFD model	CLE model	BLE model
Aggregate modulus (MPa)	0.415 ± 0.248	$0.438 \pm 0.253^*$	$0.451 \pm 0.228^{*+}$
Fiber modulus (MPa)	0.288 ± 0.209	$1.519 \pm 1.099^*$	/
Permeability ($10^{-15} \text{m}^4 / (\text{N} * \text{s})$)	5.041 ± 2.154	5.597 ± 3.559	$4.626 \pm 2.322^+$
R-squared	0.988 ± 0.014	0.988 ± 0.013	$0.781 \pm 0.082^{*+}$

The permeability determined from the curve-fits is $5.597 \pm 3.559 \times 10^{-15} \text{m}^4 / (\text{Ns})$, $5.041 \pm 2.154 \times 10^{-15} \text{m}^4 / (\text{Ns})$ and $4.626 \pm 2.322 \times 10^{-15} \text{m}^4 / (\text{Ns})$ for the CLE, CFD and BLE models, respectively. A significant difference is only detected between the CLE and BLE models ($p = 0.007$). Similar to the aggregate moduli, the permeability values from the three models are highly correlated with each other in a linear relationship ($r > 0.96$) (Fig. 4.6b, 4.7b). As the fiber moduli in the two nonlinear models have different physical meanings, their magnitudes are not comparable with each other, but nevertheless they are linearly correlated ($r = 0.98$) (Fig. 4.6c).

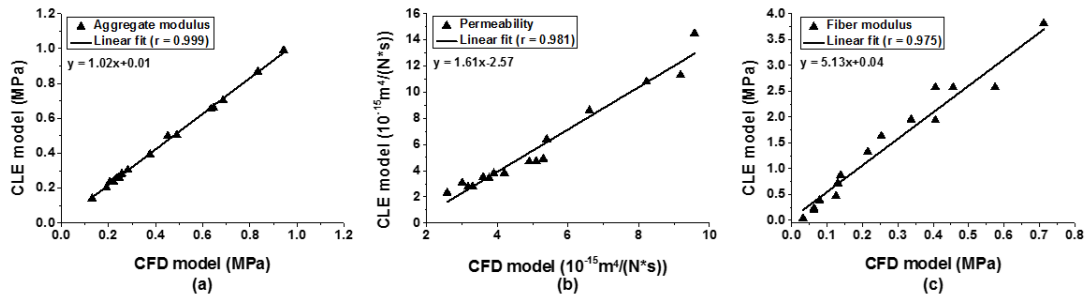


Figure 4.6 Correlations between mechanical properties determined by biphasic CLE and CFD models. (a) Aggregate modulus, (b) permeability, and (c) fiber modulus.

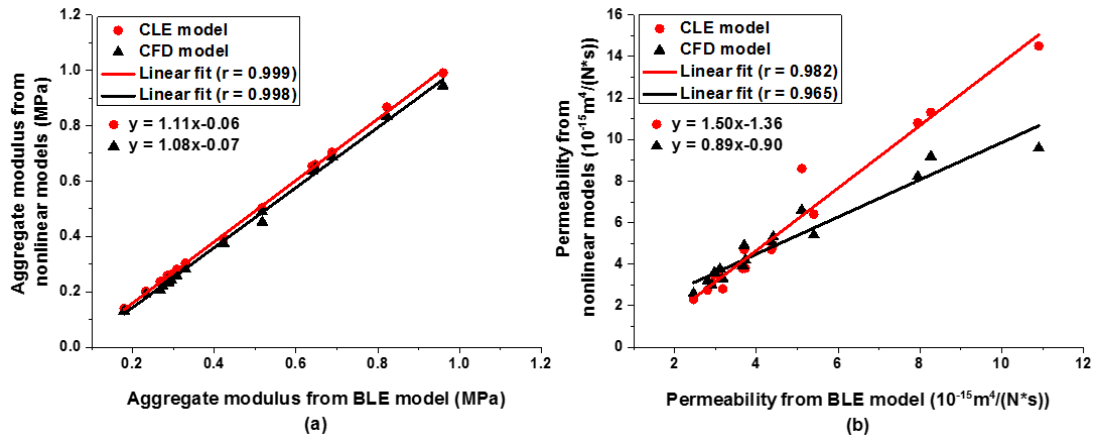


Figure 4.7 (a) Aggregate modulus and (b) permeability obtained from CLE and CFD models are linearly correlated with those from the BLE model.

To evaluate the effect of different Poisson's ratios of the solid matrix background on the outcome of our curve-fitting program, a parametric study was performed by varying the Poisson's ratio from 0 to 0.45 (Fig. 4.8). Over this range, the R-squared value of the curve-fitting varies from 0.996 to 0.998, indicating that the assigned magnitude of Poisson's ratio has little effect on the goodness of curve-fit. When the Poisson's ratio is varied from 0 to 0.15, the calculated permeability and

fiber modulus change 5% and 7%, respectively, and the aggregate modulus increases by 1%.

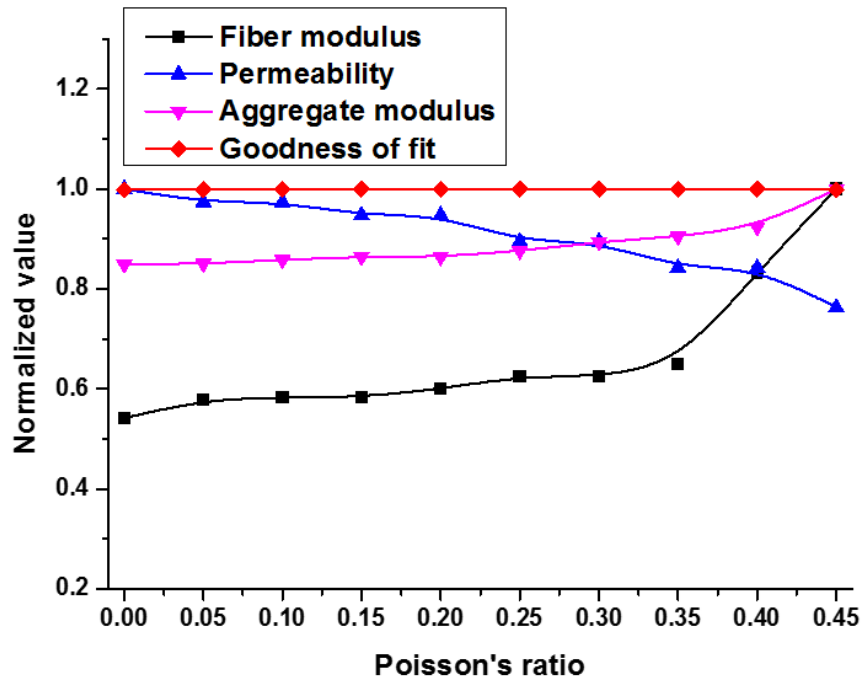


Figure 4.8 Curve-fitting is performed with different Poisson's ratios of the ground matrix on a single creep curve, and its effect on the determined mechanical properties is plotted. All the mechanical properties are normalized by their maximum value.

4.4 Discussion

In the present study, the uniqueness of the curve-fit is a result of the distinct role that each of the three mechanical properties plays in shaping the simulated creep curve. The monotonic correlations between the curve characteristics and the mechanical properties shown in the parametric studies (Fig. 4.2 and 4.3) contribute to this uniqueness and improve the efficiency of the optimization. An essential

observation that makes this curve-fitting technique viable is that variation in the permeability only shifts the half deformation time of the simulated creep curve along the logarithmic time scale. The same phenomenon has been noted previously and served as an important constraint in the indentation curve-fitting program based on the BLE model. Our current study shows that this useful phenomenon is retained when tension-compression nonlinearity is incorporated into the constitutive law. Moreover, the permeability values determined from the curve-fitting based on the BLE and CFD models (Table 4.1) displayed no statistical difference, which implies that the permeability in linear and nonlinear models may play similar, if not identical, roles in controlling the cartilage response under indentation.

The compressive moduli from the two nonlinear models are highly correlated with the modulus from the classic BLE model ($r > 0.998$), which helps confirm the accuracy of the FE program and the curve-fitting strategy. The determined mechanical properties of the bovine trochlear groove cartilage are consistent with other experimental measurements as well, which showed the aggregate modulus and the permeability to be 0.37 ± 0.02 MPa and $\sim 10^{-15}$ m⁴/(Ns) respectively. In addition, the aggregate moduli from the CLE and CFD models are linearly correlated to each other with a slope close to 1, which confirms that the compressive modulus in the two nonlinear models are comparable with each other.

It should be noted that the tensile parameters in the two models have very different physical meanings. The fiber modulus ζ is correlated nonlinearly with the tensile modulus of the cartilage measured in the experiments, which itself is strain-dependent [37, 39]. According to the correlation in Eq. 4.4, the CLE model gives an approximate tensile modulus of 6 MPa in this study, which is consistent with the

physiological range of adult bovine knee cartilage [46, 47]. However, the tensile modulus of the superficial tangential zone in cartilage has been shown to be approximately 2 times higher than that in the middle-deep zone [19]. Since the deformation field in cartilage under large-scale indentation is heterogeneous, with higher tensile strains in the superficial layer, the tensile property determined by indentation could be affected more by the superficial tangential zone rather than the deep zone cartilage. The fiber modulus ζ in the CFD model has an implicit correlation with the engineering tensile modulus. Due to the continuous angular distribution of fibers, unidirectional tension will induce different levels of stretching among the fibers oriented in different directions. Therefore, the fiber modulus ζ has drastically different physical meaning in two models, and should only be compared directly with the values obtained from the same model as indicated previously [39]. For healthy hyaline cartilage, the CFD model has been shown to explain the observed tissue behaviors, especially the strain-dependent Poisson's ratio, better than the CLE model [39]. Consequently, the CLE model is more suited for some fibrous cartilage tissues with collagen fibers uniformly aligned in one or two directions, such as meniscus [48], the superficial zone of cartilage [49] and some fibrous cartilage [50, 51].

The effective compressive Poisson's ratio of cartilage as a whole, measured directly by optical techniques [18, 31-33], is inherently small for a tension-compression nonlinear material, because the high tensile modulus confines the expansion of the tissue in the lateral direction. Since the tensile modulus is nonlinearly strain-dependent, the measured effective Poisson's ratio demonstrates a similar trend [18, 39]. The effective Poisson's ratio is higher at small compressive strains and sharply decreases to a value close to zero (~ 0.03) as the compressive strain becomes

higher than 4% [18]. The Poisson's ratio used in both the CLE and CFD models, however, is assigned to the non-fibril ground matrix. Therefore the value chosen should be slightly higher than the tissue's effective Poisson's ratio [37]. Since there is no existing measurement of this parameter, it has been assumed to be somewhere between 0 and 0.15 in literature [21, 24, 37]. Since Poisson's ratio decreases significantly from the deep zone to the superficial zone of cartilage [33] and the indentation response of cartilage is primarily regulated by the top layer, its value was fixed at 0 for this study.

A number of limitations in this study should be noted. First, the two nonlinear constitutive models employed are based on the continuum assumption, *i.e.*, the basic assumption of porous elastic theory, which assumes there is a mixture of solid and fluid phases in any infinitesimal small volume. Since commercial nano-indenters have recently become readily available, nano-indentation has been widely used for the characterization of cartilage [5, 13, 52]. When the indenter size is on the same scale as collagen fibrils or chondrocytes [53], the continuum assumption is no longer valid, and the technique developed here is therefore not suitable for estimation of mechanical properties at the nano-scale. Secondly, articular cartilage has a much more complicated structure than that described by the two nonlinear models here. For example, the collagen fibers are organized heterogeneously across the cartilage, mainly aligned in the horizontal directions in the superficial zone and vertically in the deep zone. The hydraulic permeability is anisotropic and nonlinearly dependent on the dilatation of the solid matrix. In addition, the osmotic pressure induced by negatively charged proteoglycans contributes to the compressive stiffness. None of these is accounted for in the two tension-compression nonlinear models. Furthermore, the

intrinsic viscoelasticity of the solid matrix, which is a key factor regulating the short-term response of cartilage [54], is not considered in the two constitutive models. As the contribution of the intrinsic viscoelasticity is lumped into the elastic properties of solid matrix, the tensile moduli determined using the CLE and CFD models may be an overestimation and higher than the actual values. Therefore, although the two current models can describe the overall transient mechanical behaviors of cartilage better than the linear isotropic theory, they represent simplifications of the real structure of the tissue. Thirdly, the tensile modulus in the nonlinear model can significantly affect the initial deformation or “jump” of the creep curve. To be consistent, we defined this “jump” at a specific time after the step loading. A parametric study showed that any time in the range of 1-15 seconds gave identical curve-fitting results. This selection disappears if a ramp loading is employed, in which case the initial jump can be defined as the deformation at the end of the loading phase.

Chapter 5

SUMMARY AND FUTURE DIRECTIONS

5.1 Summary

In this thesis, a novel technique based on PCA was developed, which can predict the full indentation creep curve based on the first few minutes of deformation history. Furthermore, an efficient curve-fitting technique was developed which can uniquely and simultaneously determine the tensile modulus, compressive modulus and permeability of cartilage based on a single indentation creep curve. The new curve-fitting program can easily be applied for various experimental loading profiles, e.g. step loading, ramp loading and some specific loading functions. In addition, the type and geometry of indenter tip could also be easily adjusted in the program.

5.2 Future directions

The material behavior of articular cartilage has been studied in detail for decades. Anisotropy, inhomogeneity and tension-compression nonlinearity of the cartilage are now well-understood [30]. However, the 3D modeling of the tissue is still simplified in terms of both geometry and constitutive relations [5, 25]. The deviation between the computational model and natural tissue makes the simulation less reliable in clinical applications [55]. A current trend is to build patient specific finite element models from imaging techniques such as CT or MRI. However, current techniques do not have enough resolution to provide sufficient signal-to-noise ratio for constructing accurate 3D models. In addition, the model construction process can take tremendous efforts finishing segmentation and mesh generation. The difference in time scale between clinical application and modeling requirements, and the inability of the

current imaging technology to provide sufficient resolution for constructing accurate subject-specific 3D models are potential future directions.

REFERENCES

1. Hayes, W.C., et al., *A mathematical analysis for indentation tests of articular cartilage*. J Biomech, 1972. **5**(5): p. 541-51.
2. Jurvelin, J., et al., *Indentation study of the biochemical properties of articular cartilage in the canine knee*. Eng Med, 1987. **16**(1): p. 15-22.
3. Lu, X.L., et al., *Indentation determined mechano-electrochemical properties and fixed charge density of articular cartilage*. Ann Biomed Eng, 2004. **32**(3): p. 370-9.
4. Chen, X., B.K. Zimmerman, and X.L. Lu, *Determine the equilibrium mechanical properties of articular cartilage from the short-term indentation response*. J Biomech, 2015. **48**(1): p. 176-80.
5. Chen, X., et al., *Determining tension-compression nonlinear mechanical properties of articular cartilage from indentation testing*. Ann Biomed Eng, 2015: p. 1-11.
6. Li, Q., et al., *Biomechanical properties of murine meniscus surface via AFM-based nanoindentation*. J Biomech, 2015. **48**(8): p. 1364-70.
7. Mow, V.C., et al., *Biphasic creep and stress relaxation of articular cartilage in compression? Theory and experiments*. J Biomech Eng, 1980. **102**(1): p. 73-84.
8. Mak, A.F., W.M. Lai, and V.C. Mow, *Biphasic indentation of articular cartilage--I. Theoretical analysis*. J Biomech, 1987. **20**(7): p. 703-14.
9. Mow, V.C., et al., *Biphasic indentation of articular cartilage--II. A numerical algorithm and an experimental study*. J Biomech, 1989. **22**(8-9): p. 853-61.
10. Spilker, R.L., J.K. Suh, and V.C. Mow, *A finite element analysis of the indentation stress-relaxation response of linear biphasic articular cartilage*. J Biomech Eng, 1992. **114**(2): p. 191-201.
11. Appleyard, R.C., P. Ghosh, and M.V. Swain, *Biomechanical, histological and immunohistological studies of patellar cartilage in an ovine model of osteoarthritis induced by lateral meniscectomy*. Osteoarthr Cartilage, 1999. **7**(3): p. 281-94.
12. Bae, W.C., et al., *Indentation testing of human articular cartilage: effects of probe tip geometry and indentation depth on intra-tissue strain*. J Biomech, 2006. **39**(6): p. 1039-47.
13. Han, L., et al., *Time-dependent nanomechanics of cartilage*. Biophys J, 2011. **100**(7): p. 1846-54.
14. Guo, H. and R.L. Spilker, *An augmented Lagrangian finite element formulation for 3D contact of biphasic tissues*. Comput Method Biome, 2014. **17**(11): p. 1206-16.
15. Simha, N.K., et al., *Effect of indenter size on elastic modulus of cartilage measured by indentation*. J Biomech Eng, 2007. **129**(5): p. 767-75.

16. Athanasiou, K.A., A. Agarwal, and F.J. Dzida, *Comparative study of the intrinsic mechanical properties of the human acetabular and femoral head cartilage*. J Orthop Res, 1994. **12**(3): p. 340-9.
17. Le, N.A. and B.C. Fleming, *Measuring fixed charge density of goat articular cartilage using indentation methods and biochemical analysis*. J Biomech, 2008. **41**(3): p. 715-20.
18. Chahine, N.O., et al., *Anisotropic strain-dependent material properties of bovine articular cartilage in the transitional range from tension to compression*. J Biomech, 2004. **37**(8): p. 1251-61.
19. Huang, C.Y., et al., *Anisotropy, inhomogeneity, and tension-compression nonlinearity of human glenohumeral cartilage in finite deformation*. J Biomech, 2005. **38**(4): p. 799-809.
20. Fortin, M., et al., *Unconfined compression of articular cartilage: nonlinear behavior and comparison with a fibril-reinforced biphasic model*. J Biomech Eng, 2000. **122**(2): p. 189-95.
21. Soltz, M.A. and G.A. Ateshian, *A Conewise Linear Elasticity mixture model for the analysis of tension-compression nonlinearity in articular cartilage*. J Biomech Eng, 2000. **122**(6): p. 576-86.
22. Wilson, W., et al., *A fibril-reinforced poroviscoelastic swelling model for articular cartilage*. J Biomech, 2005. **38**(6): p. 1195-204.
23. Park, S., et al., *Cartilage interstitial fluid load support in unconfined compression*. J Biomech, 2003. **36**(12): p. 1785-96.
24. Makela, J.T., M.R. Huttu, and R.K. Korhonen, *Structure-function relationships in osteoarthritic human hip joint articular cartilage*. Osteoarthr Cartilage, 2012. **20**(11): p. 1268-77.
25. Taffetani, M., et al., *Poroviscoelastic finite element model including continuous fiber distribution for the simulation of nanoindentation tests on articular cartilage*. J Mech Behav Biomed Mater, 2014. **32**: p. 17-30.
26. Gupta, S., et al., *A fiber reinforced poroelastic model of nanoindentation of porcine costal cartilage: a combined experimental and finite element approach*. J Mech Behav Biomed Mater, 2009. **2**(4): p. 326-37; discussion 337-8.
27. Julkunen, P., et al., *A review of the combination of experimental measurements and fibril-reinforced modeling for investigation of articular cartilage and chondrocyte response to loading*. Comput Math Method M, 2013. **2013**: p. 326150.
28. Lu, X.L., V.C. Mow, and X.E. Guo, *Proteoglycans and mechanical behavior of condylar cartilage*. J Dent Res, 2009. **88**(3): p. 244-8.
29. Lu, X.L. and V.C. Mow, *Biomechanics of articular cartilage and determination of material properties*. Med Sci Sports Exerc, 2008. **40**(2): p. 193-9.

30. Mow, V.C. and X.E. Guo, *Mechano-electrochemical properties of articular cartilage: their inhomogeneities and anisotropies*. *Annu Rev Biomed Eng*, 2002. **4**: p. 175-209.
31. Jurvelin, J.S., M.D. Buschmann, and E.B. Hunziker, *Optical and mechanical determination of Poisson's ratio of adult bovine humeral articular cartilage*. *J Biomech*, 1997. **30**(3): p. 235-41.
32. DiSilvestro, M.R., et al., *Biphasic poroviscoelastic simulation of the unconfined compression of articular cartilage: I--Simultaneous prediction of reaction force and lateral displacement*. *J Biomech Eng*, 2001. **123**(2): p. 191-7.
33. Wang, C.C., et al., *An automated approach for direct measurement of two-dimensional strain distributions within articular cartilage under unconfined compression*. *J Biomech Eng*, 2002. **124**(5): p. 557-67.
34. Lai, W.M., J.S. Hou, and V.C. Mow, *A triphasic theory for the swelling and deformation behaviors of articular cartilage*. *J Biomech Eng*, 1991. **113**(3): p. 245-58.
35. Korhonen, R.K., et al., *Importance of the superficial tissue layer for the indentation stiffness of articular cartilage*. *Med Eng Phys*, 2002. **24**(2): p. 99-108.
36. Jin, H. and J.L. Lewis, *Determination of Poisson's ratio of articular cartilage by indentation using different-sized indenters*. *J Biomech Eng*, 2004. **126**(2): p. 138-45.
37. Wilson, W., et al., *Stresses in the local collagen network of articular cartilage: a poroviscoelastic fibril-reinforced finite element study*. *J Biomech*, 2004. **37**(3): p. 357-66.
38. Sokoloff, L., *Elasticity of articular cartilage: effect of ions and viscous solutions*. *Science*, 1963. **141**(3585): p. 1055-1057.
39. Ateshian, G.A., et al., *Modeling the matrix of articular cartilage using a continuous fiber angular distribution predicts many observed phenomena*. *J Biomech Eng*, 2009. **131**(6): p. 061003.
40. Jackson, J.E., *A user's guide to principal components*. Vol. 587. 2005: John Wiley & Sons.
41. Martin Bland, J. and D. Altman, *Statistical methods for assessing agreement between two methods of clinical measurement*. *The lancet*, 1986. **327**(8476): p. 307-310.
42. Athanasiou, K.A., et al., *Interspecies comparisons of in situ intrinsic mechanical properties of distal femoral cartilage*. *J Orthop Res*, 1991. **9**(3): p. 330-40.
43. Mow, V.C., W.Y. Gu, and F.H. Chen, *Structure and function of articular cartilage and meniscus*, in *Basic orthopaedic biomechanics and mechano-biology*, V.C. Mow and R. Huiskes, Editors. 2005, Lippincott Williams & Wilkins: Philadelphia. p. 181-258.

44. Kuroda, S., et al., *Biomechanical and biochemical characteristics of the mandibular condylar cartilage*. Osteoarthr Cartilage, 2009. **17**(11): p. 1408-15.
45. Maas, S.A., et al., *FEBio: finite elements for biomechanics*. J Biomech Eng, 2012. **134**(1): p. 011005.
46. Williamson, A.K., A.C. Chen, and R.L. Sah, *Compressive properties and function-composition relationships of developing bovine articular cartilage*. J Orthop Res, 2001. **19**(6): p. 1113-21.
47. Williamson, A.K., et al., *Tensile mechanical properties of bovine articular cartilage: variations with growth and relationships to collagen network components*. J Orthop Res, 2003. **21**(5): p. 872-80.
48. LeRoux, M.A. and L.A. Setton, *Experimental and biphasic FEM determinations of the material properties and hydraulic permeability of the meniscus in tension*. J Biomech Eng, 2002. **124**(3): p. 315-21.
49. Ruggiero, L., et al., *Roles of the fibrous superficial zone in the mechanical behavior of TMJ condylar cartilage*. Ann Biomed Eng, 2015. **43**(11): p. 2652-62.
50. Allen, K.D. and K.A. Athanasiou, *Viscoelastic characterization of the porcine temporomandibular joint disc under unconfined compression*. J Biomech, 2006. **39**(2): p. 312-22.
51. Detamore, M.S. and K.A. Athanasiou, *Tensile properties of the porcine temporomandibular joint disc*. J Biomech Eng, 2003. **125**(4): p. 558-65.
52. Moyer, J.T., A.C. Abraham, and T.L. Haut Donahue, *Nanoindentation of human meniscal surfaces*. J Biomech, 2012. **45**(13): p. 2230-5.
53. Darling, E.M., S. Zauscher, and F. Guilak, *Viscoelastic properties of zonal articular chondrocytes measured by atomic force microscopy*. Osteoarthritis Cartilage, 2006. **14**(6): p. 571-9.
54. Huang, C.Y., et al., *Experimental verification of the roles of intrinsic matrix viscoelasticity and tension-compression nonlinearity in the biphasic response of cartilage*. J Biomech Eng, 2003. **125**(1): p. 84-93.
55. Ateshian, G.A., C.R. Henak, and J.A. Weiss, *Toward patient-specific articular contact mechanics*. J Biomech, 2015. **48**(5): p. 779-786.

Appendix A

VERIFICATION OF THE NONLINEAR MODELS

A.1 Experimental verification of the predictive ability of the nonlinear models

Three cartilage-bone blocks, without removing the superficial layer, were harvested from the tibia plateaus of calf knee joints. As similar protocol to that in the manuscript was adopted to conduct the indentation testing. First, the cartilage was preloaded with 50mN force by a flat-ended porous cylindrical indenter tip ($\phi = 2.1$ mm) for 0.5h to ensure full contact between the indenter and cartilage surface. Then a 50mN step load was applied and maintained for 1 h. After the first indentation test, the sample was left to recover for 3h. Then a second indentation test was conducted with 150mN step load at the same location on the cartilage for 1h. The thickness of the cartilage was later measured using the needle penetration method.

The creep curve generated under the 150mN load was first fitted by the CLE and CFD models, and then the cartilage's response under 50mN was predicted by the parameter set obtained from the curve-fitting. The results are shown in Fig. A.1. (CFD model generates similar results thus only results from CLE are shown).

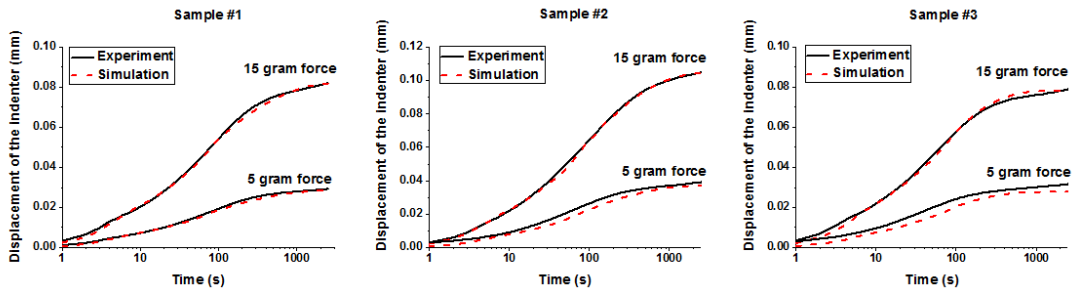


Figure A.1 Creep curves generated by 150 mN load were first fitted, and the response of cartilage under 50 mN load was predicted with the parameters obtained through curve-fitting

In general, the predictions match the experimental data, but have lower equilibrium deformations and take longer time to reach equilibrium (the curve shifts to the right). These differences are mainly due to the strain dependent permeability and modulus of the solid matrix, which are not considered in the two current models. At small strain, both the tensile and compressive moduli of the solid matrix should be lower due to the existence of a toe region in the stress-strain curves at small strain. Therefore the modulus determined under the 15 gram force loading is an over-estimation of the actual tissue modulus under 5 gram force, and the predicted deformation is smaller than the experimental data. In contrast, the permeability of the solid matrix should decrease when the matrix is compressed with negative dilatation. The permeability under the 15 gram force loading is smaller than that under the 5 gram force, and the predicted curve reaches equilibrium slower than the experimental data under 5 gram force. Moreover, the current two models did not consider the heterogeneous structure of cartilage layer, the osmotic pressure induced by proteoglycans, and the intrinsic viscoelasticity of the solid matrix. All these assumptions may affect the predictive abilities of the two models. Nevertheless, the comparison results from this extra study demonstrated the predictive predictions of these two widely used constitutive models for articular cartilage. Whether such abilities are acceptable is highly dependent on the requirements of the particular applications. Incorporation of a nonlinear stress-strain curve and strain-dependent permeability may increase the accuracy of the models with the cost of increased complexity.

A.2 Comparison with standard heuristic optimization method

To illustrate the efficiency enhancement from adopting the new optimization method, the Nelder-mead simplex method, which features a low number of evaluations, was used for comparison by analyzing the same indentation data. The number of evaluations obtained from the Nelder-mead method and our new method are compared and listed in the table below. The two methods give almost the same properties, and the compressive modulus, is shown in the table. While the simplex method takes significantly more evaluations, the mechanical properties determined from the two methods are almost the same (difference < 2%). Furthermore, in practice, several optimizations with different initial values have to be used to eliminate the potential local minima for the Nelder-mead method, which will double or triple the evaluation times.

Table A.1 The number of evaluations and compressive modulus obtained by two optimization methods are compared.

Sample	Binary search method*			Nelder-mead method	
	Compressive modulus (MPa)	No. of static evaluations**	No. of evaluations	Compressive modulus (MPa)	No. of evaluations
#1	0.503	42	36	0.495	214
#2	0.282	42	36	0.271	226
#3	0.303	42	36	0.295	155
#4	0.140	42	36	0.142	197
#5	0.263	42	36	0.258	183
#6	0.202	42	36	0.197	149
#7	0.259	42	36	0.248	233
#8	0.238	42	36	0.237	251
#9	0.236	42	36	0.233	113
#10	0.393	42	36	0.390	134
#11	0.255	42	36	0.253	183
#12	0.498	42	36	0.486	211
#13	0.659	42	36	0.666	197

#14	0.868	42	36	0.871	181
#15	0.704	42	36	0.718	148
#16	0.990	42	36	1.019	277
#17	0.654	42	36	0.669	156

* In this comparison, the error tolerance was set to 0, meaning that every search cannot be terminated early by being close enough to the target. Therefore the number of evaluations is the same across different samples.

** Static evaluation only calculate the steady-state deformation. Being a time-independent evaluation, this process only takes 1~2 seconds, which is small compared with the regular evaluation (~20s).

Appendix B

METHOD FOR COMPARING THE PRINCIPAL COMPONENTS

B.1 Two factors in PCA prediction accuracy

PCs generated from more full creep curves can provide better prediction of the long-term responses. Meanwhile, the accuracy of prediction is also proportional to the length of transient data available for reconstruction. To investigate the effects of these two factors on PCA prediction, parametric studies were performed using the TMJ data. PCA is conducted on 2 to 20 (denoted as N) full creep curves randomly selected from the 37 TMJ condyle samples, and the obtained PCs are used to predict the long-term responses of the 17 remaining samples based on their initial data in the first 300 or 600 seconds of testing. The average of the absolute values of the error between the predicted and actual equilibrium creep deformation are plotted against the numbers of full tests used to generate the PC (Fig. B.1). As expected, the error decreases as the number of full tests increases, especially at low N numbers. The improvement of accuracy diminishes as more full tests are included. No significant difference can be detected after N is larger than 12. The average error increases 2% when 300-seconds data is used for prediction instead of 600-seconds, and this gap cannot be reduced by increasing the number of full tests used to generate the PC.

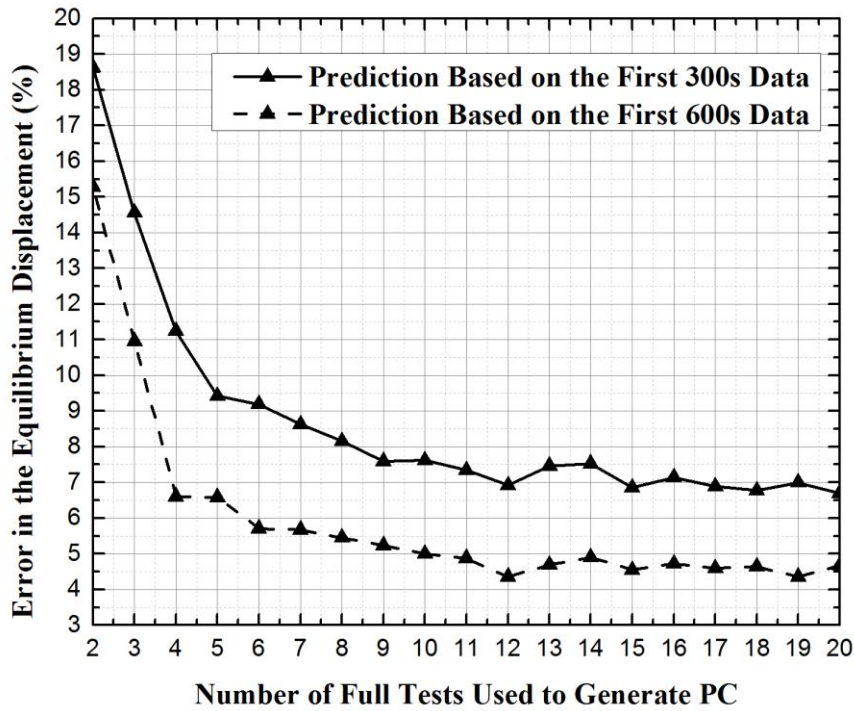


Figure B.1 The PCA prediction errors are correlated with the number of full tests used for PC matrix construction and the length of initial testing data available for prediction.

It is important to note that the result in Fig. B.1 does not necessarily suggest a minimum 12 full indentation tests for constructing the principal components. Indeed, in the present study, only 8 samples are used to extract the PC matrix for prediction. The remaining creep curves (9 knee joint creep curves, 32 TMJ creep curves) can be well predicted, and the mechanical properties obtained are consistent with those from full testing data. In the following sections, it is shown that this low number of tests can even be used to capture the regional differences in mechanical properties on the articular surface. The N number could be even smaller in practice if the requirement for precision is lower. Reasonable results can be obtained when 5 full tests were used.

As shown in Fig. B.1, the length of the base data is more important for reducing errors than increasing the number of full tests. When the first 600s of data is used, the error from merely four full tests is lower than the combination of 300s of data and 20 full tests. Therefore, if high precision is desired, such as when the difference between two comparison groups are marginally significant, a longer base data (e.g., an extra 5 minutes of testing) can be much more efficient to improve the accuracy than doing more full tests. In consideration of the constitutive assumptions in linear biphasic theory and the accuracy of biphasic curve-fitting, we recommend the N number to be 5 for most applications, which should be enough to provide reasonable prediction of the creep curves.

B.2 Comparison between principal components from two groups of samples

An important finding in this work is that PC1 is consistent within the same type of cartilage, which is the foundation of the proposed prediction technique. PC1 should represent an intrinsic pattern of the cartilage creep behavior, which could be dependent on the ultrastructure and composition of the tested tissue. Meanwhile, principal components are directly generated from the original indentation raw data, which is not affected by the assumptions in any constitutive models. Therefore, comparison of the first PC alone may reveal significant differences between the mechanical behaviors of different cartilage tissues.

B.2.1 Method

To quantitatively compare two dimensionless unit vectors, a non-parametric multivariate analysis method is introduced and tested (Anderson, Marti J. "A new

method for non-parametric multivariate analysis of variance." *Austral ecology* 26.1 (2001): 32-46.).

B.2.1.1 Create observations

To compare the PC1 between two groups of curves (e.g., curves from TMJ cartilage and knee joint cartilage), 5 curves are randomly selected from each group to generate the PCs. Fifty observations are obtained by permutation of the selection from each group, and then an observation matrix is formulated, in which each row is an observation of PC1. The first 50 rows are from group A, and the next 50 rows are from group B.

B.2.1.2 Calculate the F-ratio

The following steps are used to calculate the F-ratio:

Distance matrix D is constructed. Element d_{ij} in matrix D is defined to be the distance between observation $i=1,2,\dots,100$ and observation $j=1,2,\dots,100$. Euclidean distance is used.

Calculate the overall distance for the 100 observations from both groups:

$$SS_T = \frac{1}{100} \sum_{i=1}^{99} \sum_{j=i+1}^{100} d_{ij}^2 \quad (\text{B.1})$$

Calculate the within-group distance using the 50 observations from each group:

$$SS_W = \frac{1}{50} \sum_{i=1}^{49} \sum_{j=i+1}^{50} d_{ij}^2 \quad (\text{B.2})$$

Calculate the F-ratio:

$$F = \frac{98(SS_T - SS_W)}{SS_W} \quad (\text{B.3})$$

Note that this F ratio is based on the within-group distance and overall distance.

B.2.1.3 Comparison

By shuffling the observation matrix by exchanging rows, i.e., the first 50 rows of matrix could include observations (PC1) from both groups, a new F-ratio can be calculated and denoted as F_{π} . The shuffling is repeated 1000 times by permutation of rows, and 1000 F_{π} values were obtained. Note that the F ratio here, called mixed F ratio, is based on the distance of 50 mixed observations and the overall distance.

Calculating the p value and performing the comparison:

$$P = (\text{No. of } F_{\pi} \geq F)/1000 \quad (\text{B.5})$$

gives a P value which represents the possibility that the F ratio based on the 50 mixed observations is larger than the F ratio based on the within-group observations. If the two groups have no difference, i.e., the 50 mixed observations (PC1) are similar with the 50 within-group observations (PC1), this possibility will be close to 0.5 or 50%. If the two groups are significantly different, this possibility will be a small value or close to 0. The significance level can be selected as necessary. Using this non-parametric multivariate analysis method, comparisons are performed between the PC1s from different tissues in the present study.

B.2.2 Results

B.2.2.1 Comparison between TMJ and knee joint samples

The F ratio based on the within-group distance is 5647.7, and the possibility that the 1000 mixed F ratio is higher than 5647.7 is 0. The PC1 from TMJ and knee joint samples are significantly different with each other.

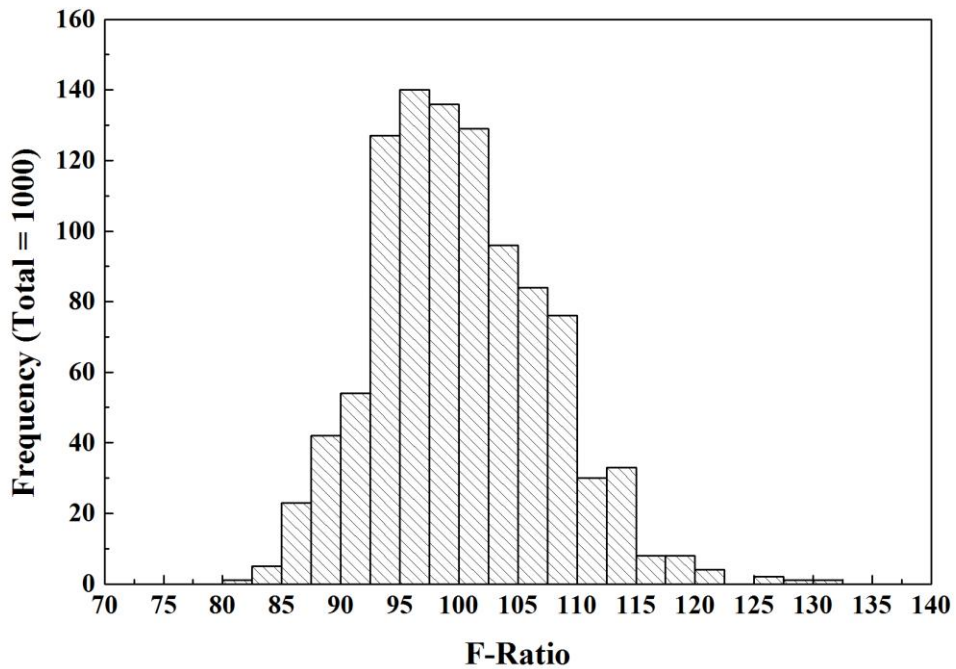


Figure B.2 Distribution histogram of the 1000 mixed F_{π} . The average of F ratio is around 100.

B.2.2.2 Comparison between randomly divided TMJ samples

For verification, the 37 TMJ samples were randomly divided into two groups, and a comparison of the PC1s of these two groups was conducted. In theory, the PC1s from the two groups should have no significant difference. The F ratio based on the within group distance is 99.1, while the possibility that the mixed F ratio is higher than 99.1 is 0.521, which is close to 0.5. The PC1s from the two groups are not significantly different. This confirms the efficiency of the non-parametric multivariate analysis in the comparison of principal components.

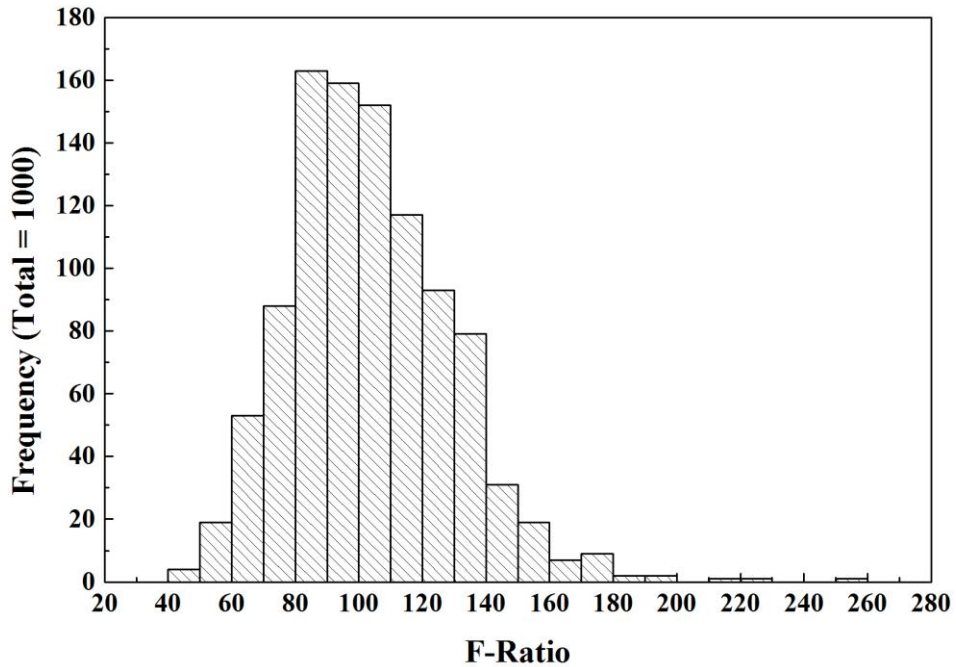


Figure B.3 Distribution histogram of 1000 mixed F_{π} .

B.2.2.3 Comparison between healthy and degenerated knee joint samples

PCA is first performed on 100 groups of creep curves, where each group includes curves from 5 healthy knee joint samples which are randomly selected from 17 samples. The average of PC1 is shown as the solid line, and the range of the 100 PC1 values is marked by the shadowed region (Fig. B.4). PCA is then performed on the creep curves from 7 degenerated samples, which were also harvested from 3-year-old adult bovine knee joint and identified as degenerated tissue using Indian ink staining. Indentation creep tests were performed on the seven samples using the same protocol as that on healthy tissue. PC1 of degenerated cartilage, shown by the dashed line, shifts significantly away from those of healthy samples. According to the non-

parametric multivariate analysis, the F ratio based on the within-group distance is 369.9, and the possibility that the mixed F ratio is higher than 369.9 is 0 (Fig. B.5). Therefore the PC1 from healthy and degenerated knee joint samples are significantly different. This example indicates that the principal components could be used as a new parameter for the comparison of mechanical behaviors between healthy and degenerated cartilages.

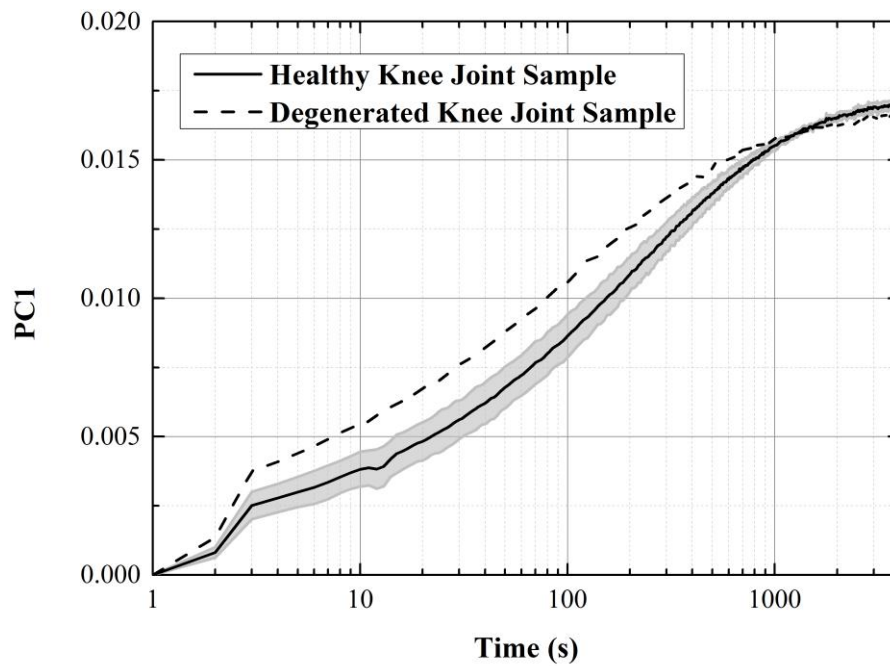


Figure B.4 The first principal component (PC1) of indentation creep curves from healthy and degenerated bovine knee cartilage.

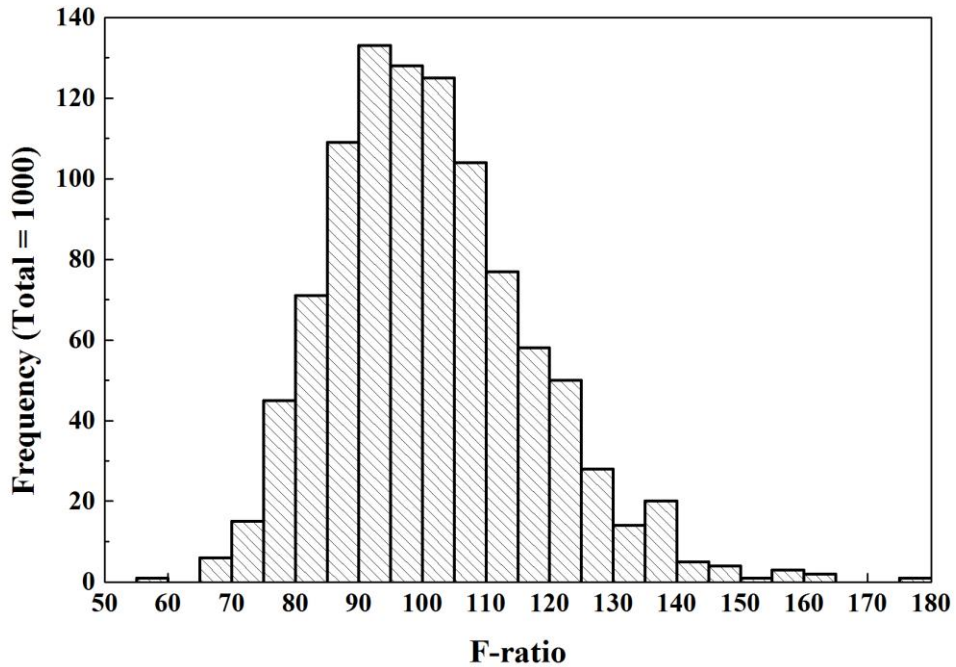


Figure B.5 Distribution histogram of 1000 mixed F_r for the comparison between healthy and degenerated knee joint samples

B.2.3 Predicting the regional difference in mechanical properties on articular cartilage

To further verify the accuracy of the PCA prediction, we revisited the data published in a previous TMJ study [28]. In this study, the creep curves of TMJ condyle cartilage were generated by 2 gram force instead of 20 gram force. Five regions on the condyle surface were indented. The principal components are first obtained from 8 randomly selected full tests which could belong to any of the five regions. For all the other tests, the full creep curves were predicted based on 600-second data using the PCs. The absolute value of errors in the predicted equilibrium deformation is 4.2%, while the average error is 0.4%. Biphasic curve fitting was

performed on all the predicted curves to obtain the mechanical properties. The aggregate moduli at five regions are summarized in Fig. B.6, side by side with the values from full indentation data. The two sets of aggregate moduli are consistent with each other, and the trend between the different regions was preserved. Results from further statistical analysis are summarized in Table B.1. The two sets of data demonstrated the same regional difference. Therefore, the PCA prediction successfully preserved the regional difference in mechanical properties on the same articular surface. The result also demonstrated that in this particular situation, for cartilage from the same joint surface, different sets of PC components are not required for the prediction of creep curves at different sites.

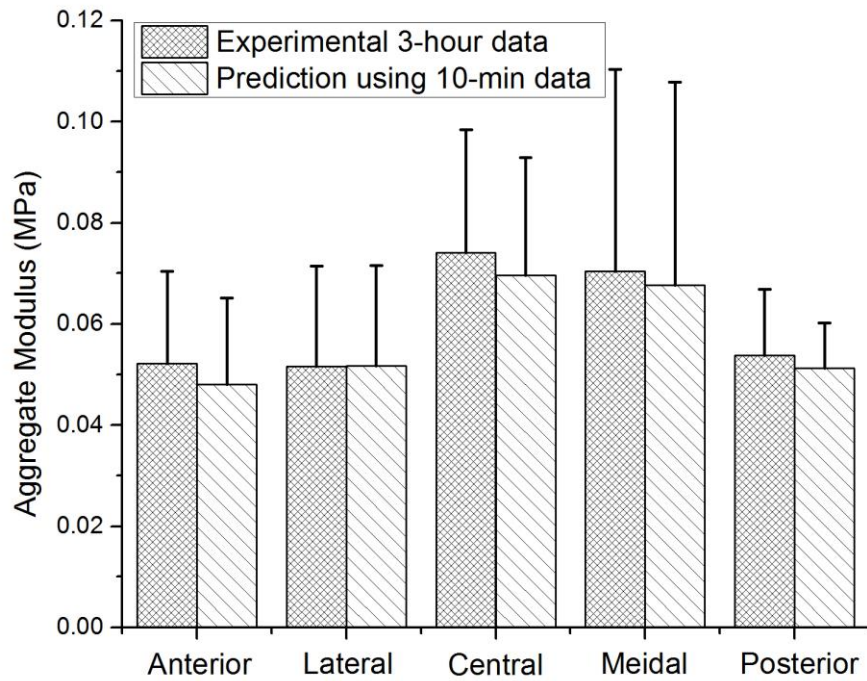


Figure B.6 Aggregate modulus from the TMJ indentation test data presented in [28]. The moduli were obtained by biphasic curve-fitting the full experimental data and PCA predicted creep data.

Table B.1 Paired t-test results of three groups: anterior & central, lateral & central, anterior and medial.

	Anterior & Central	Lateral & Central	Anterior & Medial
Experiment	P = 0.0048	P = 0.0016	P = 0.0921
Prediction	P = 0.0049	P = 0.0057	P = 0.0972